The Prandtl–Ishlinskii Hysteresis Model: Fundamentals of the Model and Its Inverse Compensator

MOHAMMAD AL JANAIDEH, MOHAMMAD AL SAAIDEH, and XIAOBO TAN

Hysteresis is a nonlinear phenomenon arising in diverse fields such as mechanics, biology, electronics, and economics [1] (see "Summary"). In particular, hysteresis is ubiquitously exhibited by various smart materials, such as piezoelectrics, magnetostrictives, and shape memory alloys [2], [3]. These materials show inherent coupling between mechanical properties and electrical/magnetic/thermal fields; therefore, they can be used as sensors and actuators. For different smart material applications, hysteresis is a main source of nonlinearity, which creates challenges in the control of these systems.

Proper modeling of the hysteresis is essential for the effective mitigation of its impact. Hysteresis models are categorized mainly into physics-based models and phenomenological models. Physics-based models aim to capture the physics of hysteresis in a particular material or system, an example of which is the Jiles–Atherton model for ferromagnetic hysteresis [4]. Phenomenological models, on the other hand, aim to describe hysteresis through mathematical representations, and they could take the form of differential equations or operators. Examples of differential equation-type hysteresis models include the Dahl model [5], the Duhem model [6], [7], and the Bouc–Wen model [8]. Operator-based models include the Prandtl–Ishlinskii (PI) model (see "Prandtl–Ishlinskii (PI) Model"); the Preisach model [9], [10], [11]; the Krasnoselskii–Pokrovskii model [12], and the Maxwell-slip model [13]. The operator-based models have been extensively used in the adaptive control [14], [15], [16], [17], [18], [19], [20], [21], [22], [23] and robust control [24], [25], [26], [27] of systems with hysteresis.

Among different hysteresis models, the PI model and its variants, including the classical PI operator, the generalized PI (GPI) operator [28], and their modifications [29], [30], have been particularly popular. For example, they have been used in the modeling of a wide range of motion control systems, as actuated by smart materials (for example, piezoelectric actuators [31], [32], [33]; magnetostrictive actuators [34]; and vanadium dioxide actuators [30]), pneumatic artificial muscles [35], and cable-driven mechanisms [36]. Reasons for the wide adoption of the PI models include their simplicity and flexibility in characterizing unsaturated and saturated hysteresis nonlinearities [28], [29].

Another particularly important reason is that, under mild assumptions, the PI models admit analytical inverses [34], which enables the efficient implementation of feedforward inverse compensation to mitigate the hysteresis effect. The PI model has been implemented within different closed-loop control systems, for instance, proportional-integral-derivative control of shape memory alloy actuators [37], adaptive control of a piezoelectric actuator [38], robust control of a piezoelectric cantilever [33], disturbance observer-based hysteresis compensation [39], dynamic inversion [40], and a hybrid switching system with a play hysteresis operator [41]. This note

- presents the mathematical formulation and the main properties of the play operator, PI model, and GPI models
- discusses the inverse of the PI model and the inverse of the GPI models

Summary

This note presents the mathematical formulations of the Prandtl–Ishlinskii (PI) and generalized PI (GPI) hysteresis models as well as their analytical inverses. These models can effectively characterize hysteresis nonlinearities in various systems, especially smart material actuators, and their inverses can be used in feedforward compensation to mitigate the effect of hysteresis. Numerical examples of the PI and GPI models as well as their analytical inverses are also included in this note. This note will introduce the PI/GPI hysteresis models to graduate students and researchers from academia and industry interested in hysteresis modeling and compensation.

Digital Object Identifier 10.1109/MCS.2023.3234381
Date of current version: 24 March 2023

1066-033X/23©2023IEEE

» outlines how the inverse of the PI model can be used as a feedforward controller for hysteresis compensation
» presents different numerical examples to simulate the characteristics of the PI model and the GPI models as well as to show the advantage of using these models within control systems.

This note is useful for graduate students, researchers, and practitioners interested in hysteresis modeling and compensation, including providing resources for the implementation of the PI models and their inverses using Matlab/Simulink. Different simulation examples are presented to support this note.

This note is organized as follows. The next section presents the classical PI model and its properties. The inverse PI model and the concept of feedforward compensation are introduced. Simulation examples are then presented. After that, GPI models based on dead-zone operators and hyperbolic tangent envelope functions as well as their inverses are presented with simulation examples. Finally, concluding remarks are provided.

THE CLASSICAL PRANDTL–ISHLINSKII HYSTERESIS MODEL AND ITS INVERSE

This section presents the PI model and its inverse. It starts with the definition of the play operator, which is the building element of the PI model. Then, the PI hysteresis model is formulated, and the main properties are introduced. The inverse of the PI model is discussed afterward.

Prandtl–Ishlinskii (PI) Model

The Prandtl–Ishlinskii (PI) model is an operator-based phenomenological scalar hysteresis model. It consists of a weighted superposition of multiple or even a continuum of elementary hysteresis units called play operators. This model can effectively characterize the hysteresis nonlinearities in diverse systems, such as actuators, motors, robots, mechanical dampers, and magnetic materials. These include the voltage-to-displacement relationship in smart material-based precise positioning actuators, the pressure–displacement curve of pneumatic artificial muscles, the stress–strain nonlinearities in mechanical dampers, and the backlash nonlinearities in robotic manipulators. Compared with other hysteresis models, the PI model has seen tremendous interest over the last two decades. This is mainly due to the simple structure of the model and the existence of its analytical inverse. The PI model and its inverse have been integrated with different control techniques to enhance the performance of actuators, robots, sensors, and motion systems. This note introduces the PI model and its generalized variants to graduate students and researchers from academia and industry who are interested in hysteresis modeling and compensation.

The Play Operator

The play operator shown in Figure 1(a) is the basic building block for the construction of the PI model. For a continuous and piecewise monotone input function $v \in C[0, T]$, where $C[0, T]$ is the space of continuous functions in the interval $[0, T]$ and an initial condition $M_0 \in \mathbb{R}$, the output of the play operator with a fixed threshold (also called the radius) of $r \geq 0$, $\Gamma_r[v, M_0] \in C[0, T]$ can be defined as follows. Let $0 = t_0 < t_1 < \cdots < t_K = T$ be a partition of the interval $[0, T]$ such that v is monotone (nondecreasing or nonincreasing) in each interval $[t_{k-1}, t_k]$, where $k = 1, \ldots, K$. Then, for $t \in (t_{k-1}, t_k]$ the output of the play operator Γ_r is defined by

$$\Gamma_r[v, M_0](t) = \max\{v(t) - r, \min\{v(t) + r, \Gamma_r[v](t_{k-1})\}\} \quad (1)$$

with initial condition

$$\Gamma_r[v, M_0](0) = \max\{v(0) - r, \min\{v(0) + r, M_0\}\}. \quad (2)$$

For ease of presentation, we write $\Gamma_r[v, M_0](t)$ as $\Gamma_r[v](t)$. The play operator is Lipschitz continuous in $C[0, T]$ in the sense that

$$|\Gamma_r[v_1](t) - \Gamma_r[v_2](t)| \leq \max_{t \in [0,T]} |v_1(t) - v_2(t)| \quad (3)$$

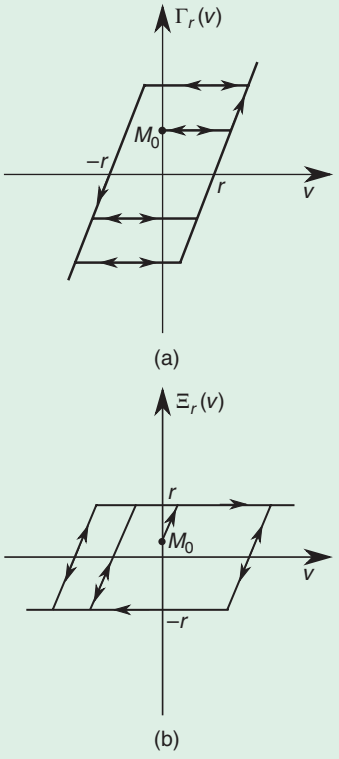

FIGURE 1 The input–output characteristic of (a) the play operator $\Gamma_r[v]$ and (b) the stop operator $\Xi_r[v]$, where v is the input, r is the threshold, and M_0 is the initial value of the output.

for all piecewise monotone functions $v_1, v_2 \in C[0, T]$ with some initial condition M_0. This enables us to extend the play operator by the density argument to the whole space $C[0, T]$. For a fixed input $v \in C[0, T]$ and time $t \in [0, T]$, when we consider $\Gamma_r[v](t)$ as a function of the threshold $r \geq 0$, it is known to be Lipschitz continuous with Lipschitz constant one [42]. As an example, the play operator can be used to model the input–output relationship of two masses, as illustrated in Figure 2(a). This figure shows that mass A and mass B move horizontally from zero initial conditions [43]. When an input force is applied to mass A, this mass will start a motion (to the right side) from $x_1 = 0$ to reach the position x_{1_m}. Mass B will stay at rest $x_2 = 0$ for $x_1 \leq a$, but it will start motion for $x_1 > a$ (to the right side) with displacement of $x_2 = x_1 - a$. As the direction of the force is reversed (to the left side), mass B will stay at the position $x_{2_m} = x_{1_m} - a$ for $x_1 > x_{1_m} - a$, and then it will start the motion (to the left side) when $x_1 < x_{1_m} - a$. This motion can be illustrated using the displacement responses for two masses, as shown in Figure 2(b). Due to this motion, the hysteresis characteristic can be observed between the displacements of two masses, as illustrated in Figure 2(c). These characteristics can be modeled using the play operator with $r = a$ and $M_0 = 0$. This behavior is also seen in spur gears and planetary gear heads, which have two engaged gears with a backlash effect.

The Stop Operator

The output of a stop operator Ξ_r, shown in Figure 1(b), is defined as [10]

$$\Xi_r[v, M_0](t) = \min\{r, \max\{-r, v(t) - v(0) + \Xi_r[v](t_{k-1})\}\} \quad (4)$$

with the initial condition

$$\Xi_r[v, M_0](0) = \min\{r, \max\{-r, v(0) + M_0\}\}. \quad (5)$$

Analytically, the output of the stop operator is bounded by the threshold r as

$$-r \leq \Xi_r[v](t) \leq r. \quad (6)$$

The stop operator can be used to study the boundedness property of the PI model.

Elastoplastic Models for the Play and Stop Operators

Elastoplastic models can be used to characterize the play operator and the stop operator [42], [44]. The elastoplastic model of the play operator consists of a parallel connection between and a rigid plastic element, as illustrated in Figure 3(a). The stop operator is represented as an elastic element connected in series with a rigid plastic element, as illustrated in Figure 3(b). The symbols σ^e and σ^p represent the elastic and plastic stress components, respectively, and the symbols ε^e and ε^p represent the elastic and plastic strain components, respectively.

The constitutive relations of the parallel elastoplastic model are given by [42]

$$\sigma = \sigma^e + \sigma^p \quad (7)$$

$$\varepsilon = \varepsilon^e = \varepsilon^p \quad (8)$$

$$\sigma^e = E\varepsilon \quad (9)$$

$$\sigma^p \in r\,\mathrm{sign}(\dot{\varepsilon}) \quad (10)$$

where E is the elasticity modulus, r is a positive constant, and "sign" is the multivalued maximal monotone sign function. The stress $\sigma(t)$ can be expressed as

$$\sigma(t) = E\varepsilon + r\,\mathrm{sign}(\dot{\varepsilon}(t)) \quad (11)$$

and the strain $\varepsilon(t)$ is expressed as

$$\varepsilon(t) = \frac{1}{E}\Gamma_r[\sigma_0^p \sigma](t) \quad (12)$$

where $\sigma_0^p = \sigma^p(0) = 0$ is the initial condition.

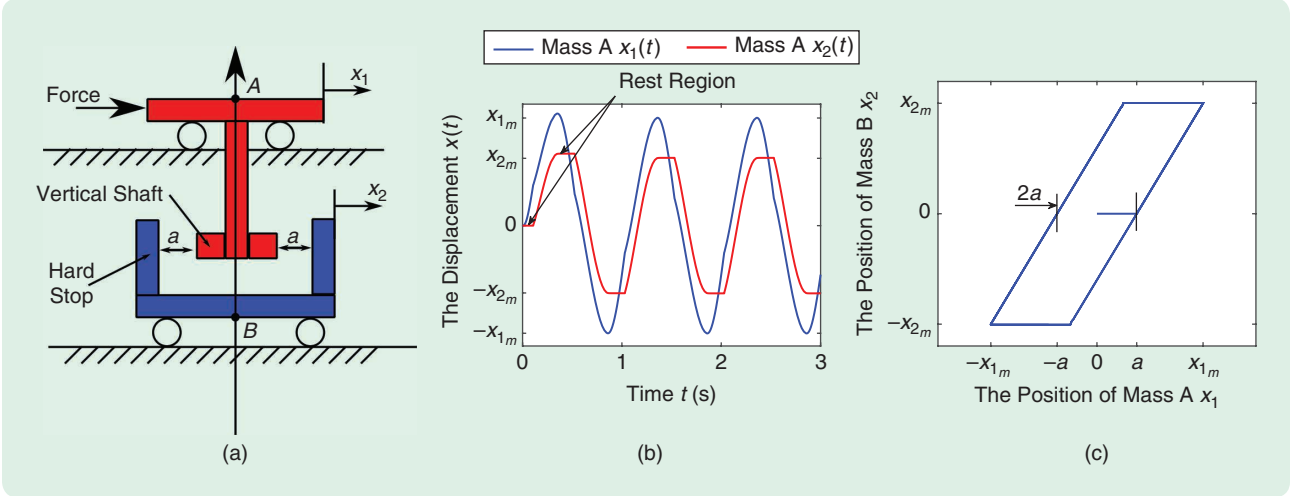

FIGURE 2 (a) A schematic diagram of two masses with a hard stop mechanism. (b) The position responses of mass A and mass B. (c) The hysteresis loop between the positions of mass A and mass B.

The constitutive relations of the series elastoplastic model are given by [42]

$$\varepsilon = \varepsilon^e + \varepsilon^p \tag{13}$$

$$\sigma = \sigma^e = \sigma^p \tag{14}$$

$$\sigma^e = E\varepsilon^e \tag{15}$$

$$\sigma^p \in r\,\mathrm{sign}(\dot{\varepsilon}) \tag{16}$$

and the stress $\sigma(t)$ can be expressed by

$$\sigma(t) = \Xi_r[\sigma_0, E\varepsilon](t) \tag{17}$$

where $\sigma_0 = \sigma(0) = 0$ is the initial condition.

The Prandtl–Ishlinskii Model and Its Properties

The PI model utilizes the play operator $\Gamma_r[v]$ and a density function $p(r)$ to describe the hysteresis nonlinearity. For a given input $v(t) \in C[0, T]$, the output of the PI model $y(t)$ is expressed analytically as [10], [33]

$$y(t) = \mathcal{P}[v](t) = p_0 v(t) + \int_0^\infty p(r)\Gamma_r[v](t)\,dr \tag{18}$$

where $p(r)$ is an integrable density function that vanishes for large values of r; namely, $p(r) = 0$ for $r > R$ for some constant R. The initial loading curve, also called the shape function, is a convex function with its derivative providing information about the shape of the PI hysteresis loops. In an analogy to mechanics of materials, the initial loading curve can be thought of as the stress–strain curve under an increasing load. For $r > 0$, the initial loading curve $\phi(r)$ can be expressed as [10]

$$\phi(r) = p_0 r + \int_0^r p(v)(r - v)\,dv \tag{19}$$

where $p(r) = \phi''(r)$; $p_0 = \phi'(0)$; and ϕ' and ϕ'' represent the first and second derivatives, respectively, of ϕ with respect to r. Consequently, the output of the PI can be presented in terms of the initial loading curve as

$$y(t) = \mathcal{P}[v](t) = \phi'(0)v(t) + \int_0^R \phi''(r)\Gamma_r[v](t)\,dr. \tag{20}$$

In practical applications since a finite number of play operators are often adequate to model the hysteresis, the PI model can be constructed by a weighted sum of n play operators $\Gamma_{r_i}[v]$, as shown in Figure 4. The output of the PI model with the thresholds satisfying $0 = r_0 < r_1 \cdots < r_n$ is expressed in a discrete form as

$$y(t) = \mathcal{P}[v](t) = p_0 v(t) + \sum_{i=1}^{n} p_i \Gamma_{r_i}[v](t) \tag{21}$$

where r_i are the thresholds of the play operators comprising the PI model with $i = 1, \ldots, n$, and $p_i \geq 0$ are the weights of the PI model. The weights and the thresholds can be identified using experimentally measured hysteresis data. For a PI model with n play operators, the initial loading curve $\phi(r)$ is piecewise linear; it can be expressed as [29], [45]

$$\phi(r) = \sum_{g=0}^{i} p_g(r - r_g), \quad \text{for } r \in [r_i, r_{i+1}), \quad i = 0, 2, \ldots, n \tag{22}$$

and its derivative has the form of

$$\phi'(r) = \sum_{g=0}^{i} p_g, \quad \text{for } r \in [r_i, r_{i+1}), \quad i = 0, 2, \ldots, n. \tag{23}$$

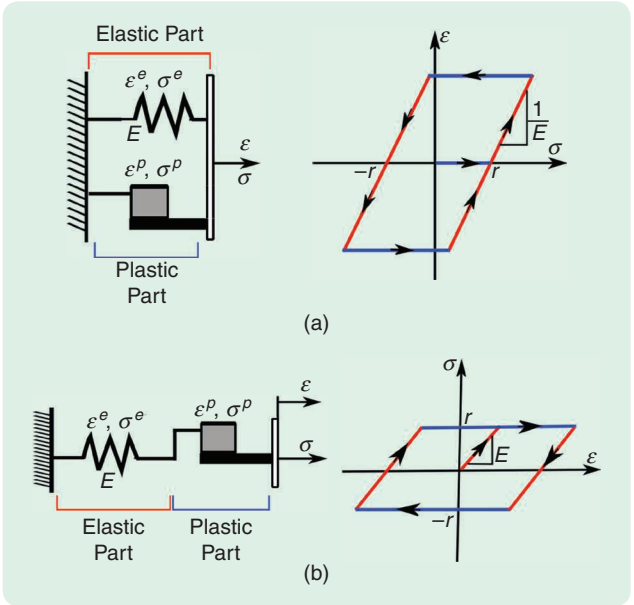

FIGURE 3 Schematic diagrams of elastoplastic model representations for (a) the play operator and (b) the stop operator.

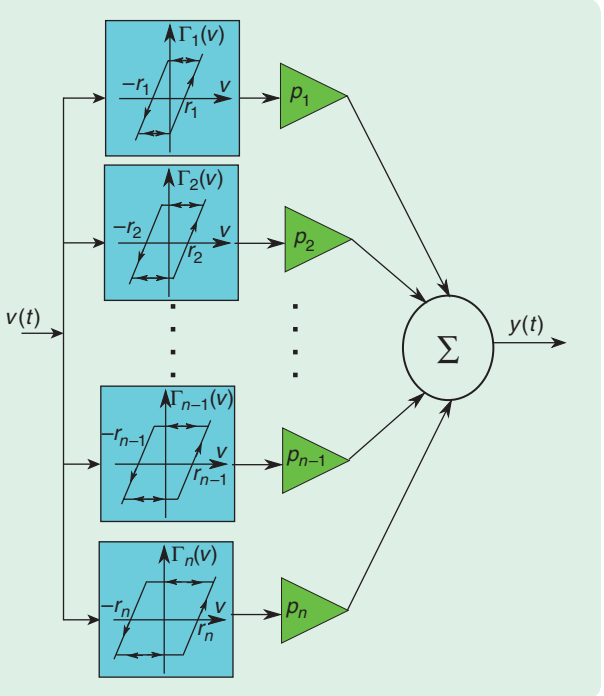

FIGURE 4 A block diagram representation of the Prandtl–Ishlinskii model.

For an arbitrary input $v(t)$, the output of the PI model $y(t)$ is illustrated in Figure 5(a), and Figure 5(b) shows the hysteresis loop between the input and the output. The properties of the PI model are summarized as follows:

» *Lipschitz continuity*: Since the play operator Γ_r is Lipschitz continuous with respect to r, the PI model is also Lipschitz continuous with respect to $(r_1, \ldots, r_i, \ldots, r_n)$ for a given input $v(t) \in C[0, T]$ [42].

» *Rate independence*: The output–input graph of the PI model is invariant to how fast the input is varied, particularly if $\psi : [0, T] \to [0, T]$ is a continuous, increasing function such that $\psi(0) = 0$ and $\psi(T) = T$. Then [10], [43],

$$\Gamma_r[v \circ \psi](t) = \Gamma_r[v](\psi(t)) \tag{24}$$

where $\circ$ denotes the composition of functions, which implies

$$\mathcal{P}[v \circ \psi](t) = \mathcal{P}[v](\psi(t)). \tag{25}$$

» *Boundedness*: The output of the play operator $\Gamma_r[v](t)$ and that of the stop operator $\Xi_r[v](t)$ with input $v(t)$ and threshold r satisfy [10]

$$\Xi_r[v](t)) + \Gamma_r[v](t) = v(t). \tag{26}$$

Since $|\Xi_r[v](t))| \le r$, it can be easily shown that the play operator output satisfies [10]

$$|v(t) - \Gamma_r[v](t)| \le r \tag{27}$$

which implies

$$|\Gamma_r[v](t)| \le |v(t)| + r \le v_{\max} + r_{\max} \tag{28}$$

where $v_{\max} = \max\{|v(t)|\}$, $r_{\max} = \max\{r\}$. The output of the PI model is given by

$$y(t) = p_0 v(t) + \sum_{i=1}^{n} p_i \Gamma_{r_i}[v](t) \tag{29}$$

which implies

$$\begin{aligned} |y(t)| &\le |p_0 v(t)| + \left| \sum_{i=1}^{n} p_i \Gamma_{r_i}[v](t) \right| \\ &\le p_0 |v(t)| + \left| \sum_{i=1}^{n} p_i v(t) \right| + \left| \sum_{i=1}^{n} p_i r_i \right|. \end{aligned} \tag{30}$$

With (28), it can be shown that

$$|y(t)| \le (p_0 + n p_{\max}) v_{\max} + n p_{\max} r_{\max} \tag{31}$$

where $p_{\max} = \max\{p_i\}$.

» *Width and slopes of the PI hysteresis loop*: The maximum width of the hysteresis loop generated among all possible inputs is presented in Figure 6(a) and can be obtained as [46]

$$\sigma = 2 \frac{\sum_{i=1}^{n} p_i r_i}{\sum_{i=1}^{n} p_i}. \tag{32}$$

The segments of the hysteresis loops for the model (21) can take up to $n + 1$ different values of slope as

$$S_i = \sum_{g=1}^{i} p_{g-1}, \quad \text{for } i = 1, \ldots, n+1. \tag{33}$$

If the thresholds of the PI model are uniformly spaced with a step size $\Delta r_i = r_i - r_{i-1}$, the relationship

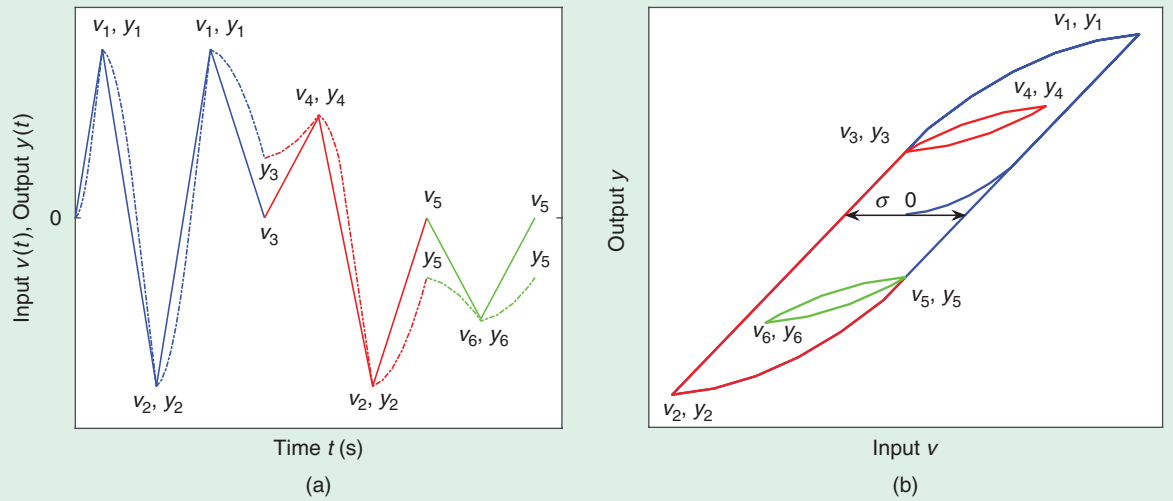

FIGURE 5 The characteristics of the Prandtl–Ishlinskii (PI) model: (a) the time signals of the input $v(t)$ (solid line) and the output $y(t)$ (dashed line) and (b) the hysteresis loop between input v and output y of the PI model (21).

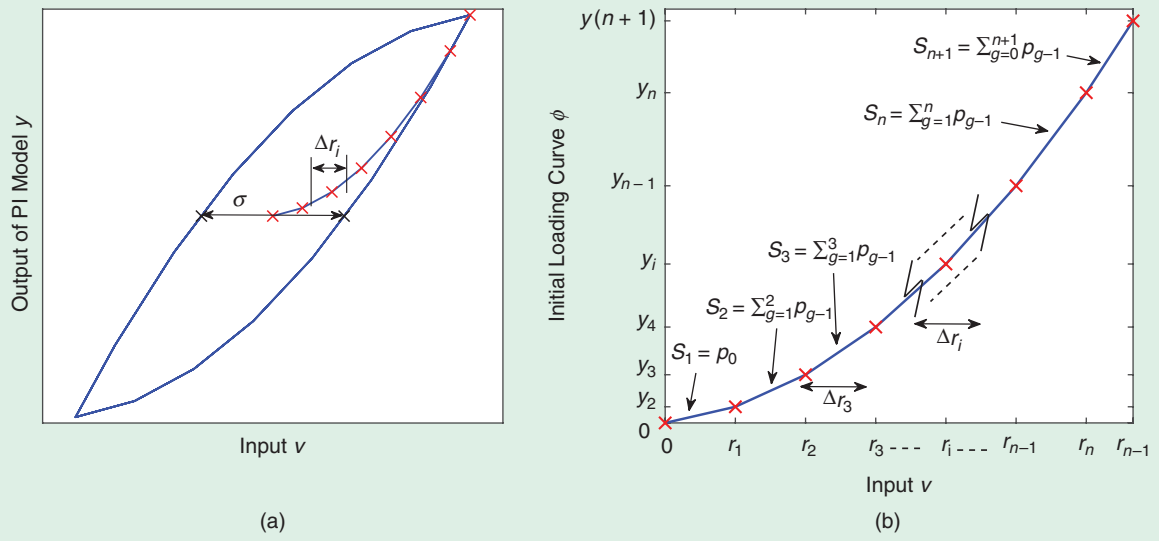

FIGURE 6 (a) The hysteresis loop between the input v and the output y, where $\Delta r_i = r_{i+1} - r_i$ $(i = 1, 2, \ldots, n)$ with $r_{n+1} = v_{\max}$. (b) The relationship between the weights p_i and the slopes S_i of the initial loading curve for n thresholds.

between the slopes of the initial loading curve and the weights are represented as shown in Figure 6(b) according to (22) and (23).

» *Inverse model*: The inverse of the PI model is exact, and it can be determined analytically. Please see the next section.

The inverse of the Prandtl–Ishlinskii model

The inverse of the PI model can be constructed analytically. In particular, it is another PI model with parameters that are functions of the parameters of the original PI model [28]. This inverse can be used as a feedforward compensator, as shown in Figure 7, to cancel the hysteresis effect of the PI model. For a reference input $u(t)$, the output of the PI model under the feedforward hysteresis compensation is

$$y(t) = \mathcal{P}[v](t) = \mathcal{P} \circ \mathcal{P}^{-1}[u](t) = u(t). \tag{34}$$

The output of the inverse PI model (control input) is given as

$$v(t) = \mathcal{P}^{-1}[u](t) = q_0 u(t) + \sum_{i=1}^{n} q_i \Gamma_{z_i}[u](t) \tag{35}$$

where Γ_{z_i} is a play operator with threshold z_i, and q_i is the associated weight. With the thresholds r_i and weights p_i of the original PI model, the thresholds z_i and weights q_i of the inverse PI model can be determined analytically as

$$z_i = \sum_{g=0}^{i} p_g (r_i - r_g) \text{ for } i = 0, \ldots, n \tag{36}$$

$$q_0 = \frac{1}{p_0}, \quad q_i = -\frac{p_i}{\left(p_0 + \sum_{g=1}^{i} p_g\right)\left(p_0 + \sum_{g=1}^{i-1} p_g\right)}, \text{ for } i = 1, \ldots, n. \tag{37}$$

In reality, the measured hysteresis loop is modeled using an approximate model $\hat{\mathcal{P}}$. The inverse model is, thus, presented as $\hat{\mathcal{P}}^{-1}$ instead of $\mathcal{P}^{-1}$. Consequently, the inverse compensation approximately rather than completely cancels out the hysteresis, resulting in some error between the y and the reference input u.

SIMULATION EXAMPLES FOR THE PRANDTL–ISHLINSKII MODEL

In this section, three numerical examples are presented to simulate the characteristics of the PI model and its inverse. Example 1 shows the characteristics of the PI model with $n = 6$. The inverse of this PI model is presented in Example 2. Example 3 shows the characteristics of the PI model in Example 1 and its inverse under an input with multiple frequencies.

Example 1

In this example, a PI model $\mathcal{P}$ with six play operators $(n = 6)$ is defined by the thresholds of $r_i = \{0.45, 0.9, 1.35,$

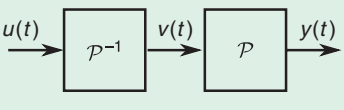

FIGURE 7 The feedforward hysteresis compensation with the inverse Prandtl–Ishlinskii (PI) model, where $u(t)$ is the reference input, $v(t)$ is the output of the inverse of the PI model, and $y(t)$ is the output of the compensation.

1.8, 2.25, 2.7} and the weights of $p_0 = 0.72$ and $p_i = \{0.6, 0.48, 0.36, 0.24, 0.12, 0.012\}$, where $i = 1, \ldots, 6$. Consider an input $v(t) = 4\sin(2\pi t)$. Figure 8(a) shows the output $y(t)$ of the PI model under the given input $v(t)$. For the given thresholds r_i, the graphs of the corresponding play operators $\Gamma_{r_i}[v]$ in (1) are illustrated in Figure 8(b). The simulated hysteresis loop between the input $v(t)$ and the output $y(t)$ as well as the initial loading curve ϕ are illustrated in Figure 8(c) and (d), respectively. Figure 9 shows the hysteresis loop at different initial conditions $M_0 = 0$, $M_0 = 1$, and $M_0 = -1$ for all play operators. This figure illustrates that the initial condition contributes a shift of the play operator outputs and, subsequently, a shift of the PI operator during the initial transient. However, the effect of the initial condition is "erased" afterward since the total variation of the input value (the value is eight) is greater than twice the largest threshold value (the value is 5.4). The width of the hysteresis loop σ is shown in Figure 10(a), and, with (32), it is calculated as $\sigma = 1.5$. Figure 10(b) shows the relationship between the slopes of segments of the initial loading curve and the weights of the play operators. The slopes of the PI hysteresis loop for $i = 1, 2, \ldots, 6$ are calculated by (33) as $S_1 = 0.71$, $S_2 = 1.33$, $S_3 = 1.8$, $S_4 = 2.16$, $S_5 = 2.4$, $S_6 = 2.51$, and $S_7 = 2.53$.

Example 2

This example focuses on the inverse of the PI model presented in Example 1. The thresholds z_i and the weights q_i of the inverse PI model $\mathcal{P}^{-1}$ are calculated using (36) as $z_0 = 0$ and $z_i = \{0.324, 0.918, 1.728, 2.7, 3.78, 4.914\}$ as well as using (37) as $q_0 = 1.3889$ and $q_i = \{-0.6313, -0.2020, -0.0926, -0.0463, -0.0198, -0.0019\}$ for $i = 1, \ldots, 6$. With

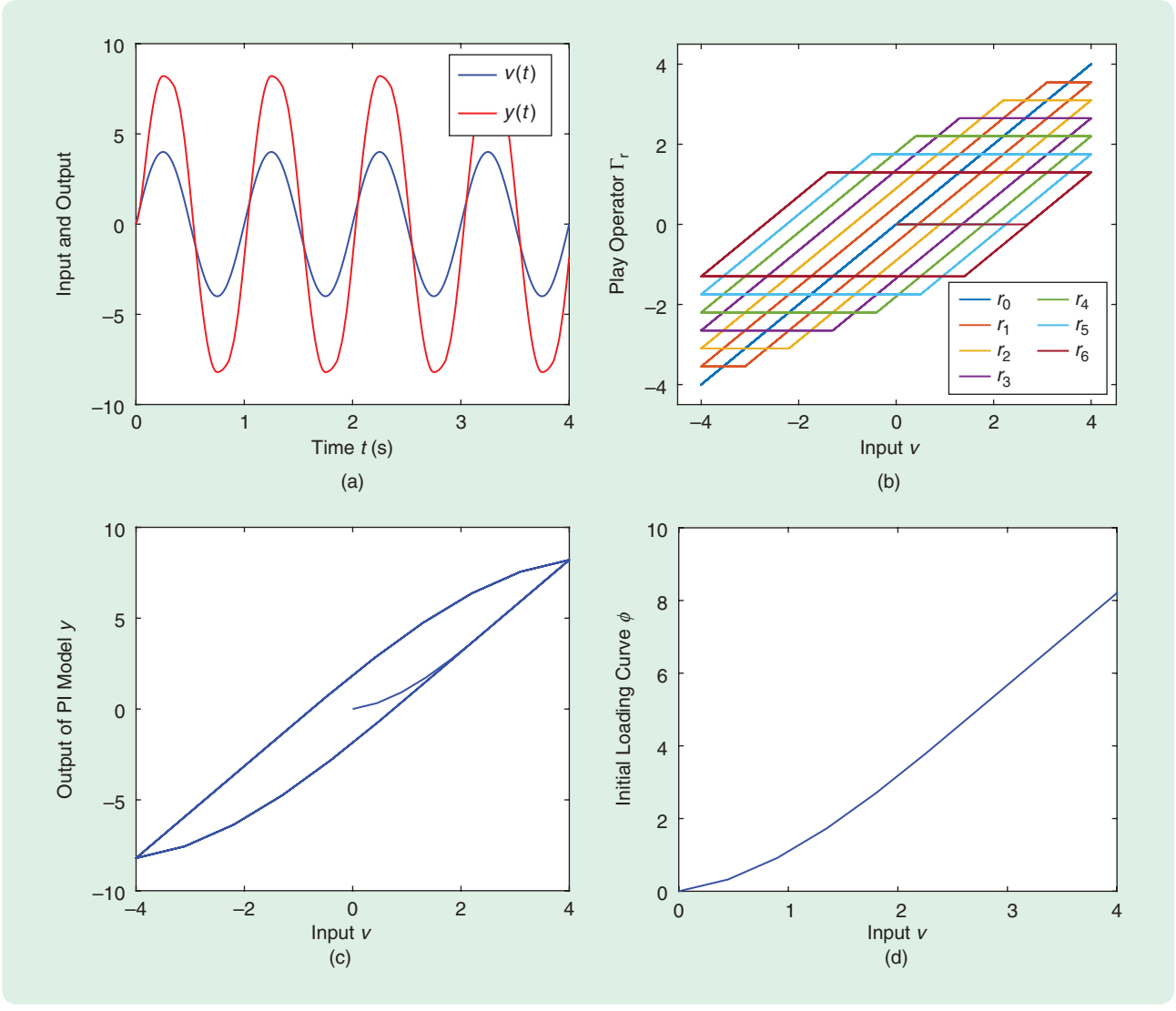

FIGURE 8 The simulation results of the Prandtl–Ishlinskii (PI) model in Example 1: (a) the input $v(t)$ and the output $y(t)$, (b) the output of the play operator $\Gamma_r[v]$ with $M_0 = 0$, (c) the simulated hysteresis loop of the PI model between the input $v(t)$ and the output $y(t)$, and (d) the initial loading curve ϕ.

a reference input of $u(t) = 10\sin(2\pi t)$, the output $v(t)$ of the inverse PI model is obtained using (35), as illustrated in Figure 11(a). For the given thresholds z_i, the graphs of the play operators $\Gamma_{z_i}[v]$ are shown in Figure 11(b). Figure 11(c) shows the hysteresis loop of the inverse PI model between the reference input $u(t)$ and the resulting $v(t)$ with the initial loading curve, as shown in Figure 11(d). Figure 12(a) and (b) shows the tracking performances between the output $y(t)$ and the reference input $u(t)$ based on the exact inverse model $\mathcal{P}^{-1}$.

Next, we consider errors in estimating PI model parameters, where the estimated thresholds are $\hat{r}_i = \{0.4678, 0.9178, 1.3678, 1.8178, 2.2678, 2.7178\}$, and the estimated weights are $\hat{p}_0 = 0.7536$, $\hat{p}_i = \{0.6192, 0.4835, 0.3637, 0.2464, 0.1410, 0.0184\}$. Thus, the thresholds and weights of the approximate inverse PI model $\hat{\mathcal{P}}^{-1}$ are calculated as $\hat{z}_0 = 0$ and $\hat{z}_i = \{0.3525, 0.9703, 1.8056, 2.8045, 3.9144, 5.0877\}$ as well as $\hat{q}_0 = 1.327$ and $\hat{q}_i = \{-0.5985, -0.1897, -0.0883, -0.0450, -0.0219, -0.0027\}$. Figure 13(a) and (b) shows the tracking performances via the comparison between the output $y(t)$ and the reference input $u(t)$ when feedforward hysteresis compensation based on the approximate inverse model $\hat{\mathcal{P}}^{-1}$ is used.

Example 3

In this example, the hysteresis loops of the PI model and its inverse are obtained for an input with two frequencies. Here, we use the parameters of the PI model given in Example 1 and a reference input of $u(t) = 5.85\sin(2\pi f_1 t) + 2.35\sin(2\pi f_2 t)$ with frequencies $f_1 = 1$ Hz and $f_2 = 5$ Hz. Figure 14(a)

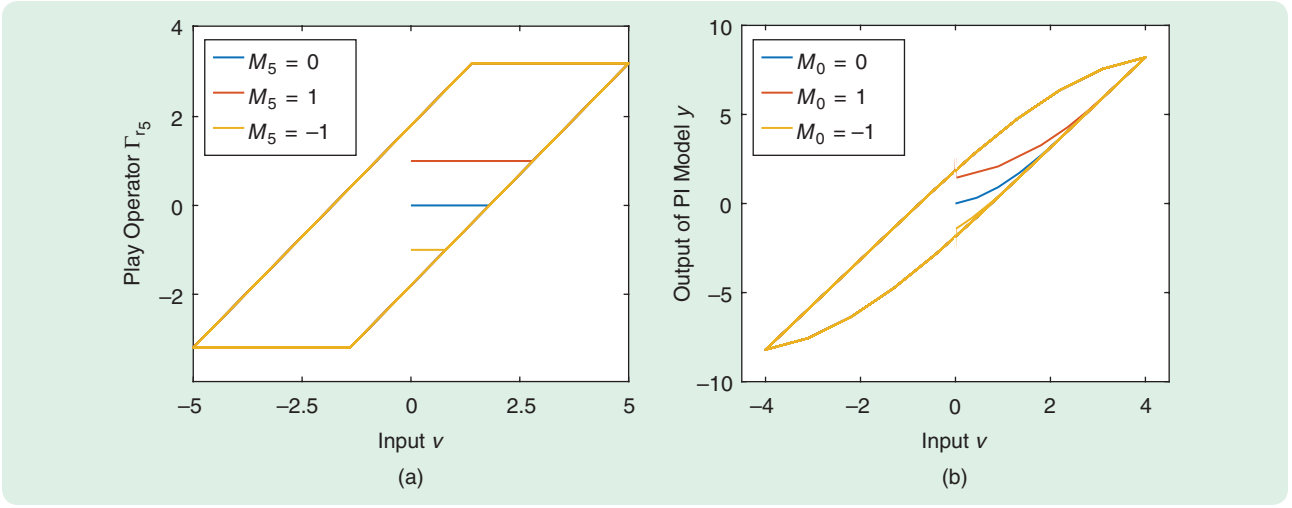

FIGURE 9 The simulation results of the Prandtl–Ishlinskii model in Example 1 with different initial conditions $M_0 = 0$, $M_0 = 1$, $M_0 = -1$ for all play operators: (a) the output of the play operator $\Gamma_{r_5}[v]$ with different values of initial condition M_0 and (b) the hysteresis loop between input $v(t)$ and output $y(t)$ corresponding to different initial conditions.

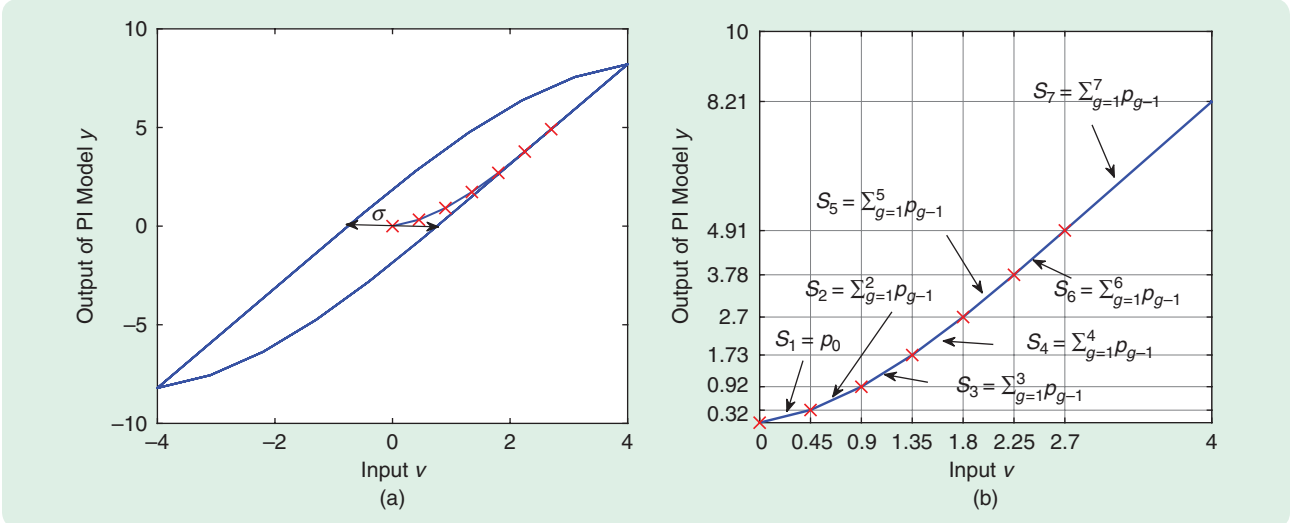

FIGURE 10 The simulation results of the Prandtl–Ishlinskii model in Example 1: (a) the hysteresis loop between the input v and the output y and (b) the relationship between the slopes of the initial loading curve and the weights.

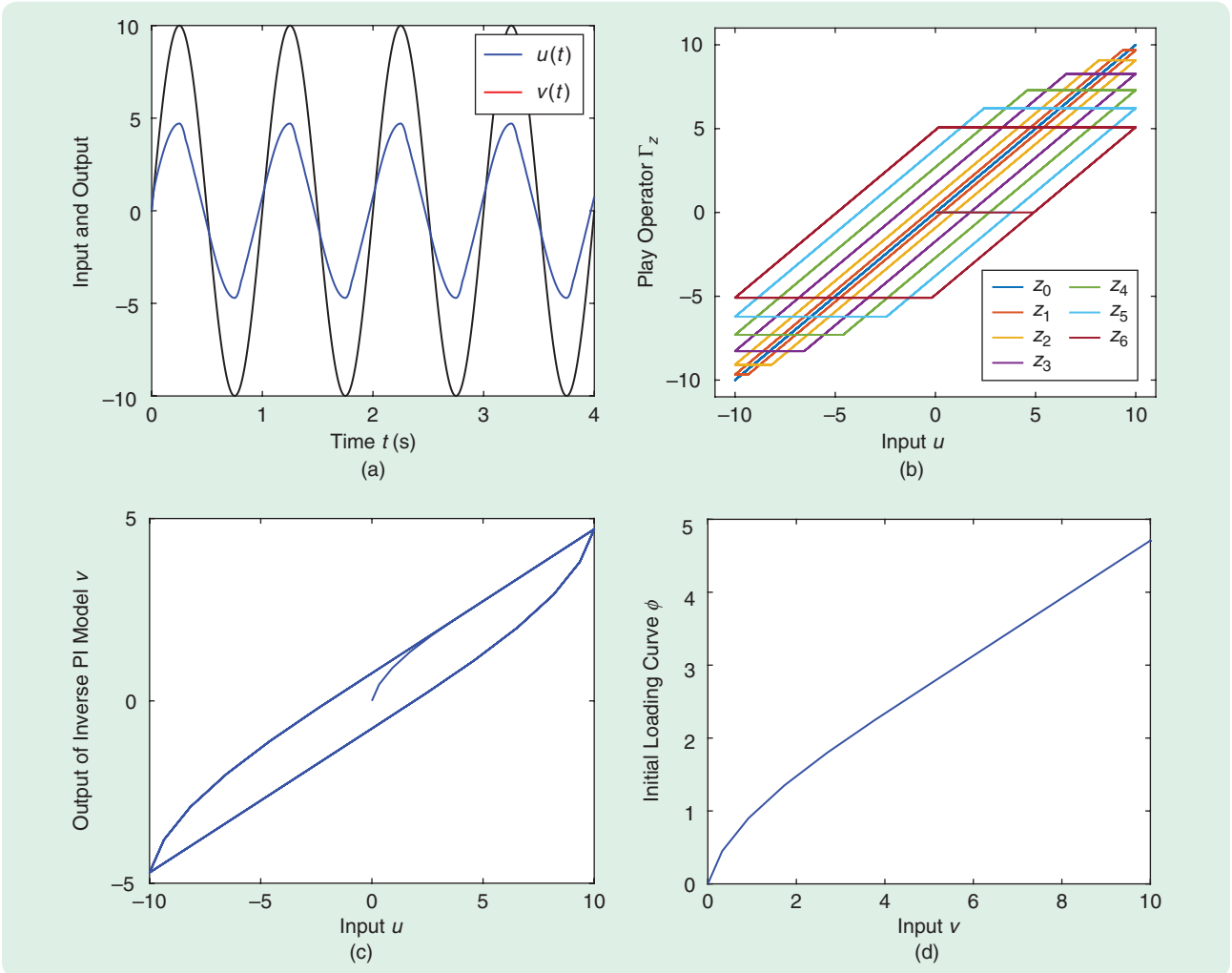

FIGURE 11 The simulation results of the inverse Prandtl–Ishlinskii (PI) model in Example 2: (a) the reference input $u(t)$ and the inverse output $v(t)$, (b) the output of the play operators $\Gamma_z[u]$ in the inverse PI operator, (c) the hysteresis loop between the reference input $u(t)$ and the inverse output $v(t)$, and (d) the initial loading curve ϕ for the inverse model.

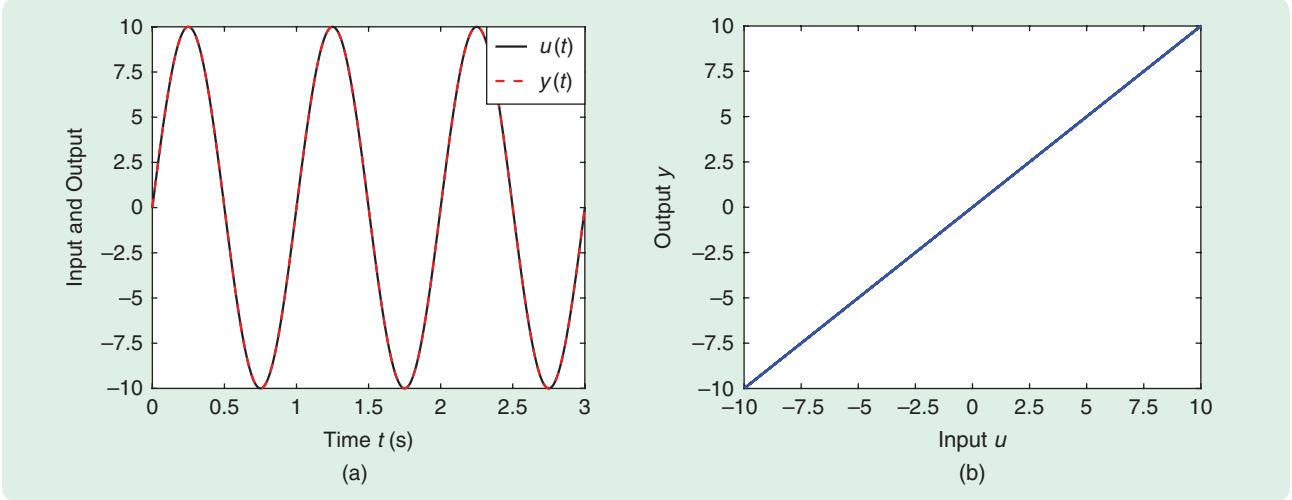

FIGURE 12 The tracking performance using the exact inverse model $\mathcal{P}^{-1}$ in Example 2: (a) the time history of the reference input $u(t)$ and the compensated output $y(t)$ and (b) the input–output characteristic upon inverse compensation.

illustrates the hysteresis loops of the inverse PI model ($\mathcal{P}^{-1}$), Figure 14(b) shows the hysteresis loops of the PI model ($\mathcal{P}$), and Figure 14(c) shows the input–output characteristic under the feedforward hysteresis compensation.

Closed-Loop Control System With Hysteresis Compensation

We now illustrate how hysteresis compensation can be used in a closed-loop control setting. The physical system with hysteresis nonlinearities can often be represented by the Hammerstein model. In particular, we consider a system consisting of the PI model $\mathcal{P}$ cascaded with a linear transfer function $G(s)$. Figure 15 represents the block diagram of the closed-loop control system with feedforward hysteresis compensation and a controller $C(s)$, where the inverse hysteresis compensator (approximately) cancels out the hysteresis effect, while the controller $C(s)$ is designed to handle the dynamics $G(s)$ and the error resulting from imperfect hysteresis inversion. Consider an example where the PI model parameters are as given in Example 1, and the transfer function $G(s)$ is given as [20]

$$G(s) = \frac{8.8 \times 10^{16}}{s^4 + 1.6 \times 10^4 s^3 + 6.6 \times 10^8 s^2 + 5.3 \times 10^{12} s + 8.8 \times 10^{16}}. \tag{38}$$

The controller $C(s)$ used is a proportional-integral controller with gains $K_p = 0.185$ and $K_i = 185$, while, for hysteresis compensation, both the exact inverse model $\mathcal{P}^{-1}$ and the approximated inverse model $\hat{\mathcal{P}}^{-1}$ obtained in Example 2 are used. Consider a reference input of $r(t) = 4\sin(2\pi t)$. Figure 16 compares the closed-loop tracking performance for three cases: without hysteresis compensation, with exact hysteresis compensation, and with approximate hysteresis compensation. It can be seen that, even with approximate inverse compensation, the closed-loop control performance is greatly improved over the case without hysteresis compensation.

It can be seen that, even with approximate inverse compensation, the closed-loop control performance is greatly improved over the case without hysteresis compensation.

GENERALIZED PRANDTL–ISHLINSKII MODELS

The GPI mode hysteresis models are formulated to characterize saturated and asymmetric hysteresis loops [28], [30], [47]. A GPI model is a cascade structure of a memoryless model with the PI model $\mathcal{P}$, as shown in Figure 17. For a given input $v(t) \in C[0, T]$, the output of GPI model $y_G(t)$ can be expressed as

$$y_G(t) = \Pi[v](t) = \mathcal{P}[w](t) = \mathcal{P} \circ \mathcal{G}[v](t) \tag{39}$$

where $w(t) = \mathcal{G}[v](t)$ is the output of the nonlinear memoryless model. The literature includes two types of memoryless models: dead-zone operator-based model (γ) [29] and nonlinear odd envelope functions (κ) [28]. It is noticed that the order of functions γ and $\mathcal{P}$ here is different from that in [29]. Lipschitz continuity of the GPI model is

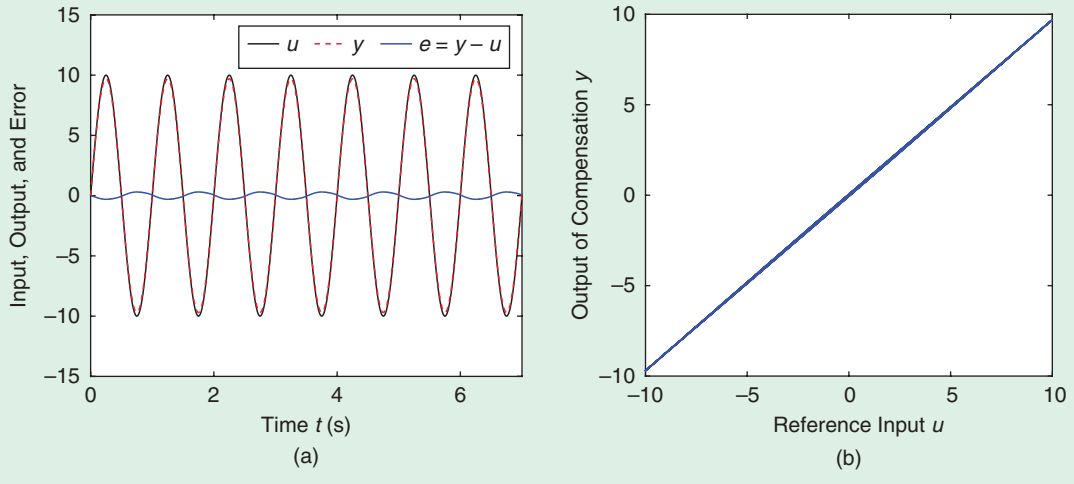

FIGURE 13 The tracking performance using an approximate inverse model $\hat{\mathcal{P}}^{-1}$ in Example 2: (a) the time history of the reference input $u(t)$ and the compensated output $y(t)$ and (b) the input–output characteristic upon inverse compensation.

ensured since the memoryless model $\mathcal{G}$ is itself Lipschitz continuous. For more details in compositions that involve hysteresis like (39), the reader can refer to [42, Sec. II.3] and [10, Sec. 2.10–2.11].

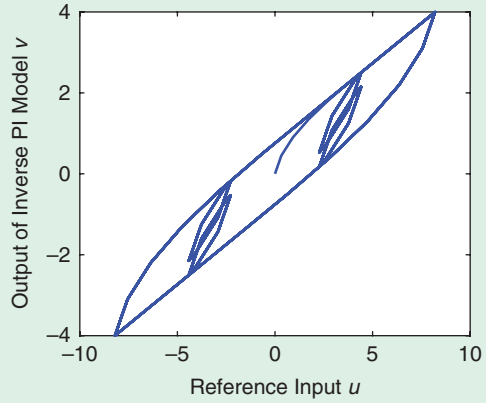

FIGURE 14 The simulation results of inverse compensation of the Prandtl–Ishlinskii (PI) model in Example 3: (a) the hysteresis loops of the inverse PI model between the reference input $u(t)$ and the inverse output $v(t)$, (b) the hysteresis loops of the PI model between the input $v(t)$ and the compensated output $y(t)$, and (c) the input–output characteristic under feedforward hysteresis compensation.

Dead-Zone Operator-Based Generalized Prandtl–Ishlinskii Model

This section introduces the dead-zone operator-based GPI model, where the memoryless model $\mathcal{G}$ is selected to be the dead-zone operator-based model γ. The output of this model can be expressed as

$$y_D(t) = \mathcal{P}[w](t) = p_0 w(t) + \sum_{i=1}^{n} p_i \Gamma_{r_i}[w](t). \tag{40}$$

As proposed in [29], [48], the output of the dead-zone superposition model is given by

$$w(t) = \gamma[v](t) = \sum_{j=-m}^{m} \eta_j \mathcal{S}_{\rho_j}[v](t) \tag{41}$$

where $\mathcal{S}_{\rho_j}$, $j = -m, \ldots, m$, are dead-zone operators, and η_j, $j = -m, \ldots, m$ are constant weights. The output of a dead-zone operator is defined as

$$\mathcal{S}_{\rho_j}[v](t) = \begin{cases} \max\{v(t) - \rho_j, 0\} & \text{if} \quad \rho_j > 0 \\ v(t) & \text{if} \quad \rho_j = 0 \\ \min\{v(t) - \rho_j, 0\} & \text{if} \quad \rho_j < 0 \end{cases} \tag{42}$$

where ρ_j are thresholds such that $\rho_{-m} < \cdots < \rho_{-1} < \rho_0 = 0 < \rho_1 < \cdots < \rho_m$. The weights η_j are selected to satisfy the monotonicity condition [48]:

$$\sum_{j=0}^{m} \eta_j > 0, \quad \text{and} \quad \sum_{j=-m}^{-1} \eta_j > 0. \tag{43}$$

Figure 18(a) illustrates the characteristic of the dead-zone operator $\mathcal{S}_{\rho_j}[v](t)$, and Figure 18(b) illustrates the output of the dead-zone superposition model $w(t)$.

Hyperbolic Tangent Function-Based Generalized Prandtl–Ishlinskii Model

This section introduces the GPI model where the memoryless model $\mathcal{G}$ is a nonlinear odd envelope function κ. One of the most popular envelope functions is the hyperbolic tangent function. The output of the hyperbolic tangent function-based GPI can be expressed as

$$y_H(t) = \mathcal{P}[h](t) = p_0 h(t) + \sum_{i=1}^{n} p_i \Gamma_{r_i}[h](t) \tag{44}$$

where $h(t)$ is the output of the hyperbolic tangent envelope function, which is defined in each interval $[t_{k-1}, t_k]$ of a partition $0 = t_0 < t_1 < \cdots < t_K = T$ as

$$h(t) = \begin{cases} \kappa_R[v](t) & \text{if} \quad v(t_k) \geq v(t_{k-1}) \\ \kappa_L[v](t) & \text{if} \quad v(t_k) < v(t_{k-1}) \end{cases} \tag{45}$$

where v is a monotone input in each interval $[t_{k-1}, t_k]$ for $k = 1, \ldots, K$. As proposed in [28] and [47], the envelope

functions in the form of the hyperbolic tangent function are given as

$$\kappa_R(v) = a_0 \tanh(a_1 v + a_2) + a_3, \tag{46}$$

$$\kappa_L(v) = b_0 \tanh(b_1 v + b_2) + b_3 \tag{47}$$

where a_0, a_1, a_2, a_3, b_0, b_1, b_2, and b_3 are constants to be identified using experimental hysteresis data. The envelope

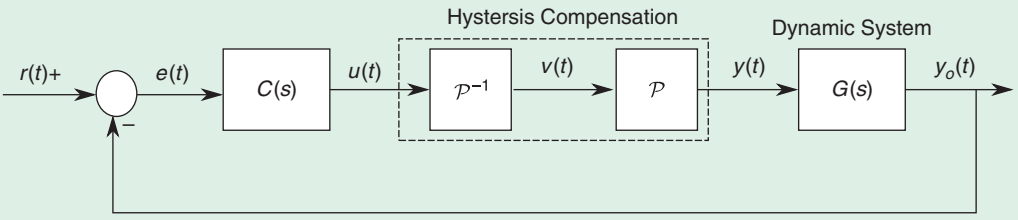

FIGURE 15 A closed-loop control system with feedforward hysteresis compensation based on the inverse Prandtl–Ishlinskii (PI) model, where $G(s)$ is the transfer function of the dynamic system, $C(s)$ is the transfer function of the controller, $r(t)$ is the reference of the output, $u(t)$ is the control signal, $v(t)$ is the output of the inverse PI model, $y(t)$ is the output of the compensation, and $y_o(t)$ is the output of the closed-loop control system.

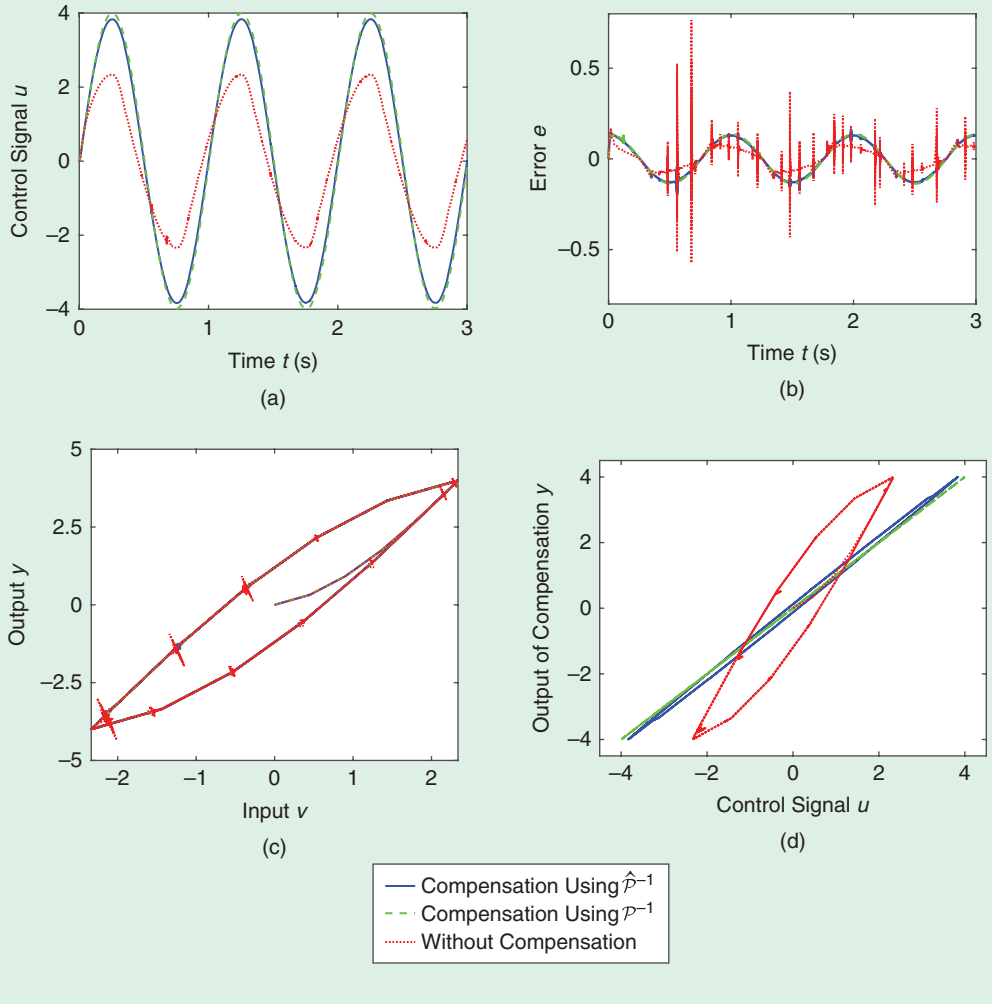

FIGURE 16 The simulation results of the closed-loop control system with hysteresis compensation and without hysteresis compensation: (a) the control signal u, (b) the tracking error $e(t) = r(t) - y_o(t)$, (c) the hysteresis loops of the Prandtl–Ishlinskii model between the input $v(t)$ and the output $y(t)$; and (d) the hysteresis loop between the control signal $u(t)$ and the compensator output $y(t)$.

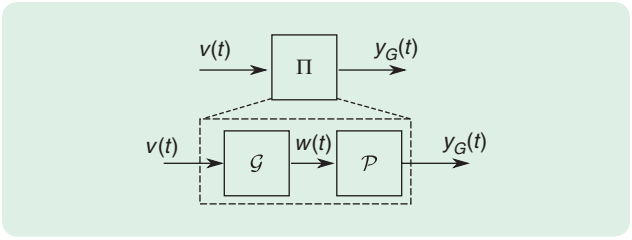

FIGURE 17 A block diagram representation of the generalized Prandtl–Ishlinskii (GPI) model Π, where $v(t)$ is the input, $\mathcal{G}$ is the memoryless model (dead-zone model γ or envelope function κ), $w(t)$ is the output of the model function, $\mathcal{P}$ is the PI model, and $y_G(t)$ is the output of the GPI model.

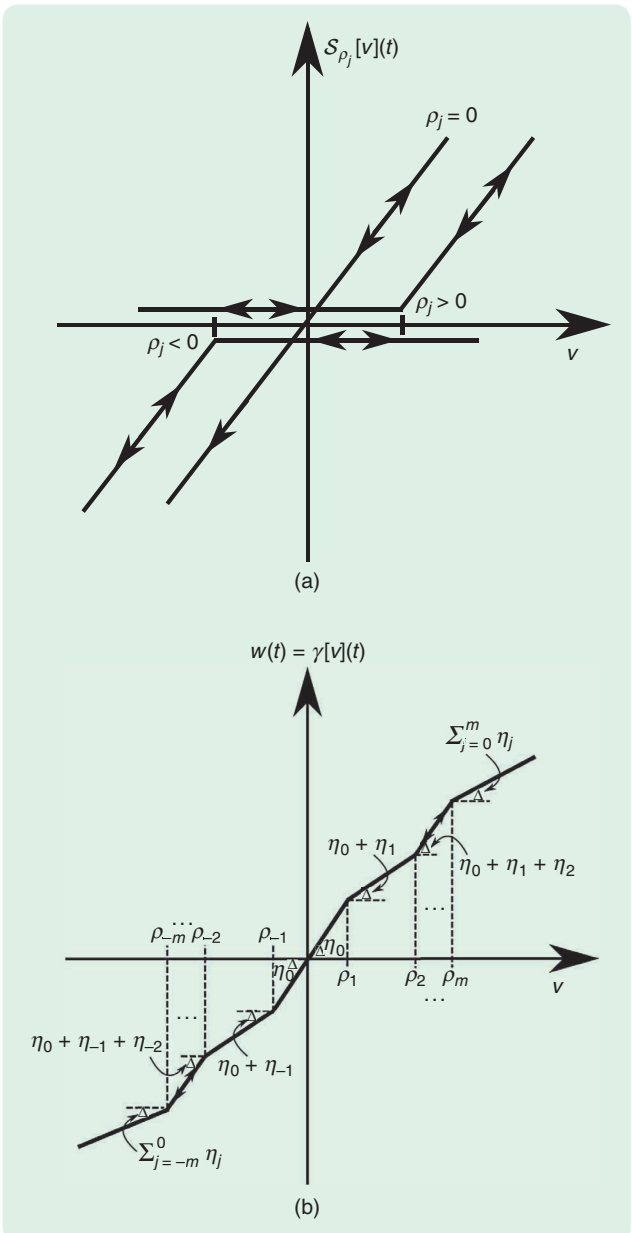

FIGURE 18 (a) The characteristic of the dead-zone operator with threshold ρ_j. (b) The output of dead-zone model with thresholds ρ_j and weights η_j, where the slope of each segment can be expressed in terms of the weights.

functions κ_R and κ_L are odd and Lipschitz-continuous functions. When $\kappa_R(v) = \kappa_L(v) = v$, the GPI model Π is reduced to the classical PI model $\mathcal{P}$.

THE INVERSE OF THE GENERALIZED PRANDTL–ISHLINSKII MODEL

The inverse GPI model can be represented as a cascade structure of the inverse memoryless model $\mathcal{G}^{-1}$ and the inverse PI model $\mathcal{P}^{-1}$, as shown in Figure 19. For a given desired input $u(t) \in C[0, T]$, the output of the inverse GPI model (control input) $v(t)$ can be expressed as

$$v(t) = \Pi^{-1}[u](t) = \mathcal{G}^{-1} \circ \mathcal{P}^{-1}[u](t) \tag{48}$$

where $u(t)$ is the reference input, $\mathcal{P}^{-1}$ is the inverse of the PI model given by (35), and $\mathcal{G}^{-1}$ is the inverse of the memoryless model. The inverse GPI model can be used as a feedforward hysteresis compensator, as shown in Figure 20, to eliminate the hysteresis effect. For a reference input $u(t)$, the output of the hysteresis nonlinearity under feedforward hysteresis compensation is

$$y_G(t) = \Pi \circ \Pi^{-1}[u](t) = (\mathcal{P} \circ \mathcal{G}) \circ (\mathcal{G}^{-1} \circ \mathcal{P}^{-1})[u](t) = u(t). \tag{49}$$

It should be noted that, in reality, an approximate model is obtained to represent the real hysteresis using the measured hysteresis data. Consequently, the inverse model consists of $\hat{\mathcal{P}}^{-1}$ and $\hat{\mathcal{G}}^{-1}$ instead of $\mathcal{P}^{-1}$ and $\mathcal{G}^{-1}$. As a result, the inverse compensation approximately instead of perfectly

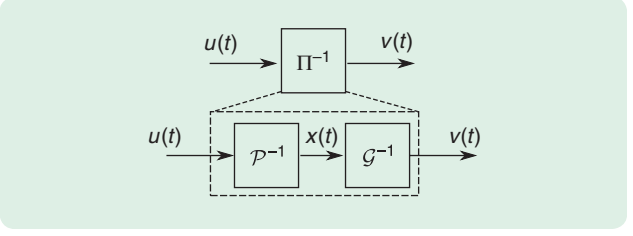

FIGURE 19 A block diagram representation of the inverse of generalized Prandtl–Ishlinskii (GPI) model, where $u(t)$ is the reference input, $\mathcal{P}^{-1}$ is the inverse of the PI model, $\mathcal{G}^{-1}$ is the inverse of the memoryless model, $x(t)$ is the output of the inverse GPI model, and $v(t)$ is the output of the inverse GPI (control input).

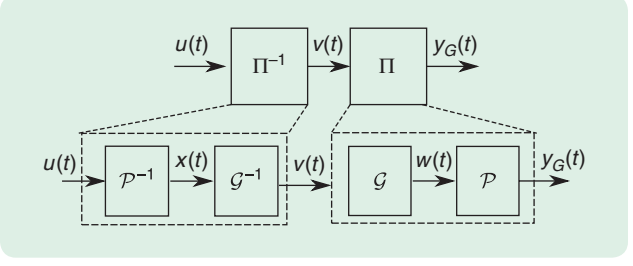

FIGURE 20 The feedforward hysteresis compensation with the inverse generalized Prandtl–Ishlinskii model, where $u(t)$ is the reference input, $v(t)$ is the control input, and $y_G(t)$ is the output.

cancels out the hysteresis, resulting in some error between the compensated output y and the reference input u.

Inverse of the Dead-Zone Operator-Based Generalized Prandtl–Ishlinskii Model

The output of the inverse γ^{-1} for the dead-zone operator-based GPI model is defined in each interval $[t_{k-1}, t_k]$ of a partition $0 = t_0 < \cdots < t_K = T$ by the formula

$$v(t) = \gamma^{-1}[x](t) = \sum_{j=-m}^{m} \mu_j \mathcal{S}_{\tau_j}[x](t) \tag{50}$$

where $\mathcal{S}_{\tau_j}$ is a dead-zone operator given by

$$\mathcal{S}_{\tau_j}(x) = \begin{cases} \max(x - \tau_j, 0) & \text{if} \quad \tau_j > 0 \\ x & \text{if} \quad \tau_j = 0 \\ \min(x - \tau_j, 0) & \text{if} \quad \tau_j < 0 \end{cases} \tag{51}$$

and $x(t)$ is the output of the inverse PI model given as

$$x(t) = \mathcal{P}^{-1}[u](t) = q_0 u(t) + \sum_{i=1}^{n} q_i \Gamma_{z_i}[u](t). \tag{52}$$

The thresholds τ_j and weight μ_j of the exact inverse dead-zone model γ^{-1} are given according to [29]. For the positive branch with $j = 0, 1, \ldots, m$, we have

$$\tau_j = \sum_{g=0}^{j} \eta_g (\rho_j - \rho_g), \quad \text{for } j = 0, 1, \ldots, m \tag{53}$$

and the weights of γ^{-1} are

$$\mu_0 = \frac{1}{\eta_0}, \quad \mu_j = -\frac{\eta_j}{\left(\eta_0 + \sum_{g=1}^{j} \eta_g\right)\left(\eta_0 + \sum_{g=1}^{j-1} \eta_g\right)}, \quad \text{for } j = 1, \ldots, m. \tag{54}$$

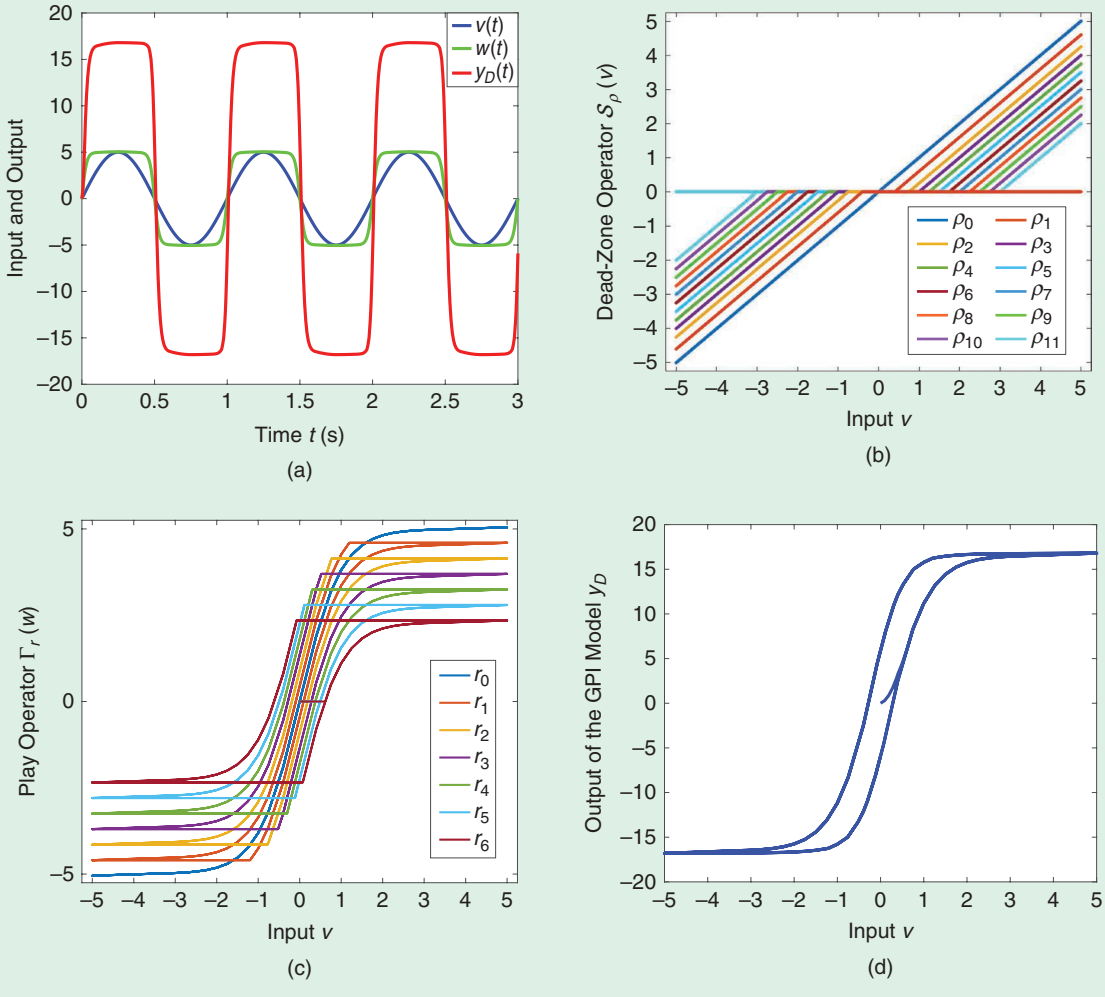

FIGURE 21 The simulation results of dead-zone operator-based generalized Prandtl–Ishlinskii (GPI) model in Example 4: (a) the input $v(t)$, the dead-zone output $w(t)$, and the output $y_D(t)$; (b) the output of the dead-zone operators $\mathcal{S}_\rho[v]$; (c) the outputs of the play operators $\Gamma_r[w]$; and (d) the input–output characteristic of the GPI mode loop between the input $v(t)$ and the output $y_D(t)$.

Similarly, for the negative branch with $j=-m,\ldots,-1$, we have

$$\tau_j=\sum_{g=j}^{0}\eta_g(\rho_j-\rho_g),\quad \text{for } j=-m,\ldots,-1 \tag{55}$$

and the weights are

$$\mu_j=-\frac{\eta_j}{\left(\eta_0+\sum_{g=j}^{-1}\eta_g\right)\left(\eta_0+\sum_{g=j+1}^{-1}\eta_g\right)},\quad \text{for } j=-m,\ldots,-1. \tag{56}$$

Inverse of the Hyperbolic Tangent Function-Based Generalized Prandtl–Ishlinskii Model

The output of the inverse κ^{-1} for the hyperbolic tangent function-based GPI model is defined in each interval $[t_{k-1};t_k]$ of a partition $0=t_0<\cdots<t_K=T$ by the formula

$$v(t)=\begin{cases}\kappa_R^{-1}[x](t) & \text{if } x(t_k)>x(t_{k-1})\\ \kappa_L^{-1}[x](t) & \text{if } x(t_k)\le x(t_{k-1})\end{cases} \tag{57}$$

where κ_R^{-1} and κ_L^{-1} are the inverse of the hyperbolic tangent envelope functions given as

$$\begin{aligned}\kappa_R^{-1}(x)&=\frac{1}{a_1}\left(\operatorname{atanh}\left(\frac{1}{a_0}(x-a_3)\right)-a_2\right)\\ \kappa_L^{-1}(x)&=\frac{1}{b_1}\left(\operatorname{atanh}\left(\frac{1}{b_0}(x-b_3)\right)-b_2\right)\end{aligned} \tag{58}$$

and $x(t)$ is the output of the inverse PI model (52).

SIMULATION EXAMPLES FOR THE GENERALIZED PRANDTL–ISHLINSKII MODEL

In this section, Examples 4 and 5 illustrate the dead-zone operator-based GPI model, and Example 6 illustrates the hyperbolic tangent function-based GPI.

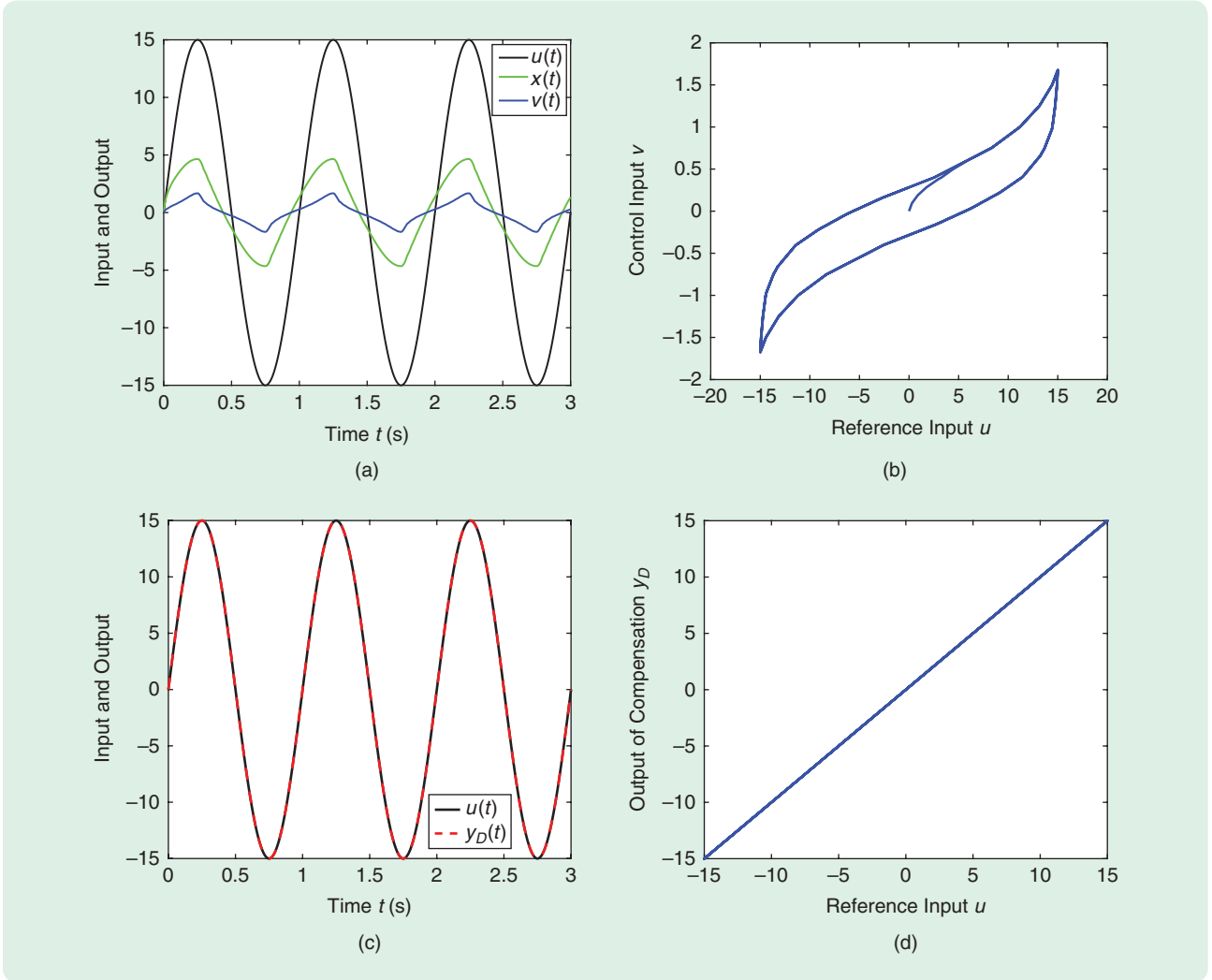

FIGURE 22 The simulation results of the inverse dead-zone operator-based generalized Prandtl–Ishlinskii (GPI) model in Example 4: (a) the reference input $u(t)$, the output of the inverse PI model $x(t)$, and the output of the inverse of the GPI model $v(t)$; (b) the hysteresis loop between the reference input $u(t)$ and the output $v(t)$; (c) the tracking performance between the reference input $u(t)$ and the compensated output $y_D(t)$; and (d) the input–output characteristic under the feedforward hysteresis compensation.

Example 4

In this example, the characteristics and hysteresis loops of the dead-zone operator-based GPI model and its inverse are obtained. For this example, consider the PI model $\mathcal{P}$ with the thresholds given as $r_i = 0.45(i)$ and the weights given by $p_i = 0.65e^{(7.75\times10^{-4})r_i}$ for $i = 0, 1, \ldots, 6$. The dead-zone operator-based model γ is assumed to have 23 elements $(m = 11)$. For the positive branch, the thresholds are $\rho_0 = 0$ and $\rho_j = \{0.4,\ 0.75,\ 1,\ 1.25,\ 1.5,\ 1.75,\ 2,\ 2.25,\ 2.5,\ 2.75,\ 3\}$ for $j = 1, \ldots, 11$. The weights are $\eta_0 = 4.765$ and $\eta_j = \{-1.128,\ -1.116,\ -0.793,\ -0.598,\ -0.413,\ -0.271,\ -0.172,\ -0.106,\ -0.066,\ -0.041,\ -0.025\}$ for $j = 1, \ldots, 11$. Considering a symmetric hysteresis loop, one can then select the thresholds and weights for $j = -11, -10, \ldots, -1$ as $\rho_{-j} = -\rho_j$ and $\eta_{-j} = \eta_j$.

For an input $v(t) = 5\sin(2\pi t)$, the dead-zone operator output $w(t)$ in (41) and the dead-zone operator-based GPI output $y_D(t)$ in (40) are illustrated in Figure 21(a). The characteristics of the dead-zone operator $\mathcal{S}_\rho[v]$ in (42) for each threshold ρ_i are illustrated in Figure 21(b). Figure 21(c) presents the outputs of the play operators Γ_r for input $w(t)$. The hysteresis loop between the input $v(t)$ and the output of the dead-zone operator-based GPI model is illustrated in Figure 21(d). The thresholds z_i and the weights q_i of the inverse PI model $\mathcal{P}^{-1}$ are calculated using (36) as $z_0 = 0$ and $z_i = \{0.293,\ 0.877,\ 1.755,\ 2.924,\ 4.386,\ 6.139\}$ as well as using (37) as $q_0 = 1.5385$ and $q_i = \{-0.7691,\ -0.2564,\ -0.1282,\ -0.0769,\ -0.0513,\ -0.0366\}$. The parameters of the inverse dead-zone operator model γ^{-1} are calculated as follows. For the positive branch with $j = 1, \ldots, 11$, the thresholds are calculated using (53) as $\tau_0 = 0$, $\tau_j = \{1.906,\ 3.179,\ 3.809,\ 4.241,\ 4.524,\ 4.704,\ 4.816,\ 4.885,\ 4.928,\ 4.954,\ 4.97\}$, and the weights are calculated using (54) as $\mu_0 = 0.210$ and $\mu_j = \{0.065,\ 0.122,\ 0.182,\ 0.305,\ 0.508,\ 0.84,\ 1.384,\ 2.248,\ 3.704,\ 6.179,\ 10.226\}$. For the negative branch with $j = -11, -10, \ldots, -1$, the thresholds and the weights are calculated as $\tau_{-j} = -\tau_j$ and $\mu_{-j} = \mu_j$, respectively.

Consider a reference input of $u(t) = 15\sin(2\pi t)$. the output of the inverse PI model $x(t)$ in (52) and the control input $v(t)$ in (50) are shown in Figure 22(a). Figure 22(b) illustrates the characteristics of the inverse dead-zone operator-based GPI model Π^{-1} between the reference input $u(t)$ and control input $v(t)$. Figure 22(c) and (d) shows the feedforward hysteresis compensation results.

Example 5

This example simulates the characteristics and hysteresis loops of the dead-zone operator-based GPI model in Example 4 under an input with multiple frequencies. For a reference input of $u(t) = 8.25\sin(2\pi f_1 t) + 6.75\sin(2\pi f_2 t)$ with frequencies $f_1 = 1$ Hz and $f_2 = 5$ Hz, Figure 23(a) illustrates the hysteresis loops of the inverse of the GPI model (Π^{-1}), Figure 23(b) shows the hysteresis loops of the GPI model (Π), and Figure 23(c) shows the input–output characteristic under the feedforward hysteresis compensation.

Example 6

In this example, the characteristics and hysteresis loops of the hyperbolic tangent function-based GPI model

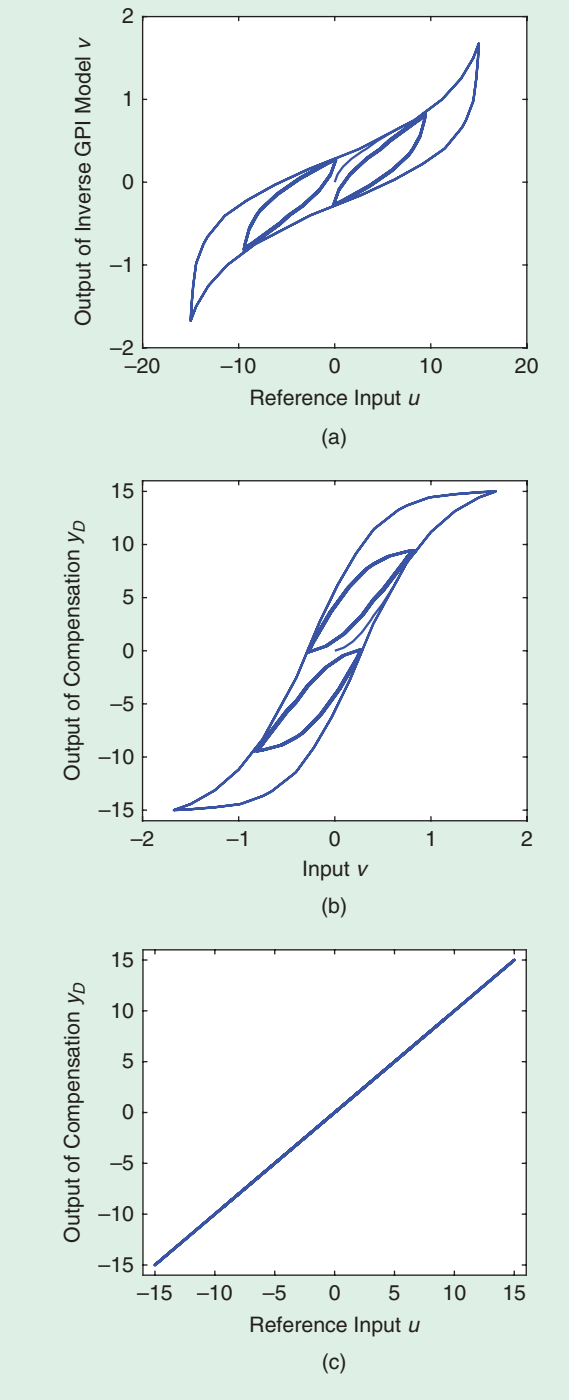

FIGURE 23 The simulation results of the dead-zone operator-based generalized Prandtl–Ishlinskii (GPI) model in Example 5: (a) the hysteresis loop of the dead-zone operator-based GPI model between the input $v(t)$ and the output $y_D(t)$, (b) the hysteresis loop of the inverse of the dead-zone operator-based GPI model between the reference input $u(t)$ and its output $v(t)$, and (c) the input–output characteristic under the feedforward compensation.

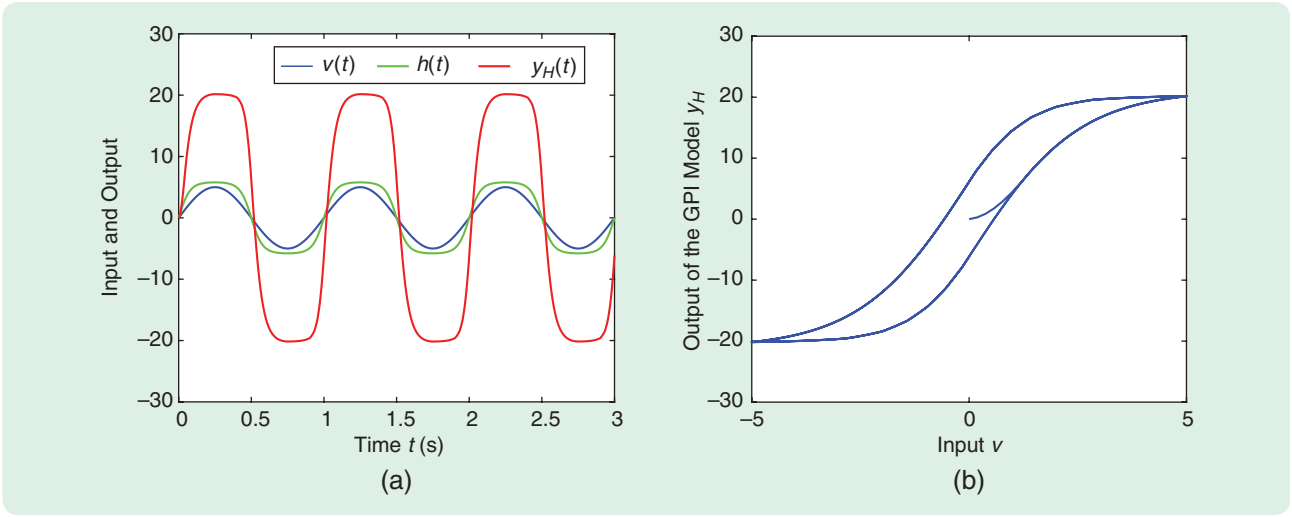

FIGURE 24 The simulation results of the hyperbolic tangent function-based generalized Prandtl–Ishlinskii (GPI) model in Example 6: (a) the input $v(t)$, the output of the hyperbolic tangent function $h(t)$, and the output $y_H(t)$ and (b) the hysteresis loop between the input $v(t)$ and the output $y_H(t)$.

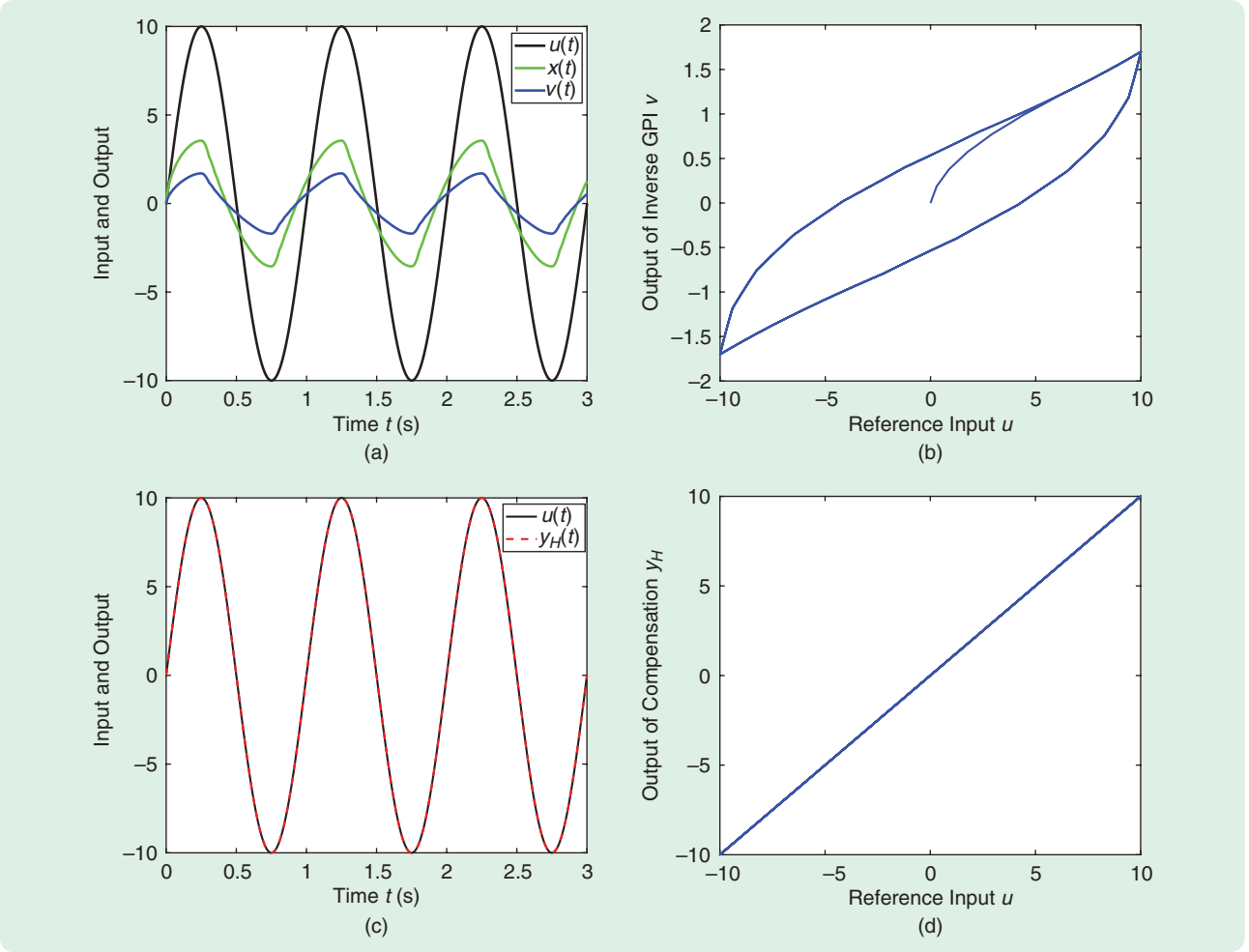

FIGURE 25 The simulation results of the inverse of the hyperbolic tangent function-based generalized Prandtl–Ishlinskii (GPI) model in Example 6: (a) the time signal of the reference input $u(t)$, the output $d(t)$, and the inverse output $v(t)$; (b) the hysteresis loop between reference input $u(t)$ and the inverse output $v(t)$; (c) the tracking between the reference input $u(t)$ and the compensated output $y_H(t)$; and (d) the input–output characteristic under feedforward compensation.

and its inverse are obtained. For this example, consider the PI model $\mathcal{P}$ with the thresholds and the weights as given in Example 4. The hyperbolic tangent envelope functions are selected as $\kappa_R = \kappa_L = 6\tanh(0.4v)$. Consider an input of $v(t) = 5\sin(2\pi t)$. Figure 24(a) shows the hyperbolic tangent envelope function output $h(t)$ in (45) and the output $y_H(t)$ in (44). The hysteresis loop between the input $v(t)$ and the output of GPI model Π is illustrated in Figure 24(b). The parameters of the inverse PI model $\mathcal{P}^{-1}$ are calculated as shown in Example 4. With (58), the inverse of the hyperbolic tangent envelope function is given as $\kappa_R^{-1} = \kappa_L^{-1} = 2.5\text{atanh}((1/6)x)$. Consider a reference input of $u(t) = 10\sin(2\pi t)$. The output of the inverse PI model $x(t)$ and the control input $v(t)$ are shown in Figure 25(a). Figure 25(b) illustrates the characteristics of the inverse of the hyperbolic tangent function-based GPI model Π^{-1} between the reference input $u(t)$ and the inverse output $v(t)$. The compensation results under the feedforward hysteresis compensation are shown in Figure 25(c) and (d).

CONCLUSION

The PI and GPI models have been widely used to characterize the hysteresis nonlinearities in smart material-based actuators. This note introduces the mathematical formulation for the PI and GPI models and their inverses. For the GPI models, examples involving both dead-zone operator-based and hyperbolic tangent function-based memoryless modules are considered. In addition, the use of the hysteresis inverse as a feedforward hysteresis compensator is discussed. Numerical examples are presented to illustrate the PI and GPI models under different input signals. The Matlab source codes to obtain the PI and GPI models for Examples 1, 4, and 6 are available at https://www.mathworks.com/matlabcentral/fileexchange/115105-prandtl-ishlinskii-hysteresis-model.

AUTHOR INFORMATION

Mohammad Al Janaideh (maljanaideh@mun.ca) received the M.A.Sc. and Ph.D. degrees in mechanical engineering (mechatronics and control) from Concordia University, Canada, in 2005 and 2010, respectively. He was a postdoctoral fellow with the Department of Electrical and Computer Engineering, University of Toronto, and the Department of Aerospace Engineering, University of Michigan, Ann Arbor. He also worked as a senior mechatronics engineer at ASML, CT, USA. Since 2017, he has been with the Department of Mechanical and Mechatronics Engineering, Memorial University of Newfoundland, Canada. His research interests include the design and control of micro- and nanopositioning systems, fault detection and mitigation of connected autonomous robotics networks, design and control of precision motion stages for semiconductor manufacturing machines, and control of systems with uncertain hysteresis nonlinearities. He is a technical editor of *IEEE Transactions on Mechatronics* and an associate editor for IEEE Conference of Decision and Control and the American Control Conference.

Mohammad Al Saaideh (maljanaideh@mun.ca) received the B.Sc. and M.Sc. degrees in electrical engineering from the University of Jordan, Jordan, in 2013 and 2020, respectively. He is with the Department of Mechanical and Mechatronics Engineering, Memorial University of Newfoundland, St. John's, NL A1B 3X5, Canada. He is working toward a Ph.D. degree in electrical engineering from Memorial University of Newfoundland. His research interests include designing and controlling micro- and nanopositioning systems; designing, developing, and controlling a reluctance actuator for a wafer scanner system in semiconductor manufacturing machines; and controlling systems with uncertain hysteresis nonlinearities.

Xiaobo Tan received the B.Eng. and M.Eng. degrees in automatic control from Tsinghua University, Beijing, China, in 1995 and 1998, respectively, and the Ph.D. degree in electrical engineering from the University of Maryland, College Park in 2002. He is currently an MSU Foundation Professor and the Richard M. Hong Endowed Chair in the Department of Electrical and Computer Engineering (ECE) at Michigan State University (MSU), East Lansing, MI 48824 USA. His research interests include modeling and control of systems with hysteresis, smart materials, underwater robotics, and soft robotics. He has been a senior editor for *IEEE/ASME Transactions on Mechatronics*. He has coauthored more than 300 peer-reviewed journal and conference papers and holds four U.S. patents. He is a Fellow of IEEE and the American Society of Mechanical Engineers (ASME) as well as a recipient of the National Science Foundation CAREER Award in 2006, MSU Teacher–Scholar Award in 2010, MSU College of Engineering Withrow Distinguished Scholar Award in 2018, and Distinguished Alumni Award from the ECE Department at the University of Maryland in 2018.

REFERENCES

[1] X. Tan and R. Iyer, "Modeling and control of hysteresis," *IEEE Control Syst. Mag.*, vol. 29, no. 1, pp. 26–28, Feb. 2009, doi: 10.1109/MCS.2008.930921.

[2] R. Smith, *Smart Material Systems: Model Development*. Philadelphia, PA, USA: Society for Industrial and Applied Mathematics, 2005.

[3] D. Leo, *Engineering Analysis of Smart Material Systems*. Hoboken, NJ, USA: Wiley, 2007.

[4] D. Lederer, H. Igarashi, A. Kost, and T. Honma, "On the parameter identification and application of the Jiles-Atherton hysteresis model for numerical modelling of measured characteristics," *IEEE Trans. Magn.*, vol. 35, no. 3, pp. 1211–1214, May 1999, doi: 10.1109/20.767167.

[5] Q. Xu and Y. Li, "Dahl model-based hysteresis compensation and precise positioning control of an XY parallel micromanipulator with piezoelectric actuation," *J. Dyn. Syst., Meas., Control*, vol. 132, no. 4, pp. 1–12, Jul. 2010, doi: 10.1115/1.4001712.

[6] R. Ouyang and B. Jayawardhana, "Absolute stability analysis of linear systems with Duhem hysteresis operator," *Automatica*, vol. 50, no. 7, pp. 1860–1866, Jul. 2014, doi: 10.1016/j.automatica.2014.04.028.

[7] J. Oh and D. Bernstein, "Semilinear Duhem model for rate-independent and rate-dependent hysteresis," *IEEE Trans. Autom. Control*, vol. 50, no. 5, pp. 631–645, May 2005, doi: 10.1109/TAC.2005.847035.

[8] F. Ikhouane, M. Victor, and J. Rodellarab, "Dynamic properties of the hysteretic Bouc-Wen model," *Syst. Control Lett.*, vol. 56, no. 3, pp. 197–205, Mar. 2007, doi: 10.1016/j.sysconle.2006.09.001.
[9] I. D. Mayergoyz, *Mathematical Models of Hysteresis and Their Applications*. New York, NY, USA: Elsevier, 2003.
[10] M. Brokate and J. Sprekels, *Hysteresis and Phase Transitions*. New York, NY, USA: Springer-Verlag, 1996.
[11] X. Tan and J. Baras, "Modeling and control of hysteresis in magnetostrictive actuators," *Automatica*, vol. 40, no. 9, pp. 1469–1480, Sep. 2004, doi: 10.1016/j.automatica.2004.04.006.
[12] M. A. Krasnosel'skii and A. V. Pokrovskii, *Systems with Hysteresis*. Berlin, Germany: Springer-Verlag, 1989.
[13] Y. Liu, H. Liu, H. Wu, and D. Zou, "Modelling and compensation of hysteresis in piezoelectric actuators based on Maxwell approach," *Electron. Lett.*, vol. 52, no. 3, pp. 188–190, Feb. 2016, doi: 10.1049/el.2015.3138.
[14] M. A. Janaideh and D. S. Bernstein, "Adaptive control of uncertain Hammerstein systems with hysteretic nonlinearities," in *Proc. 53rd IEEE Conf. Decis. Control*, Los Angeles, CA, USA, 2014, pp. 545–550, doi: 10.1109/CDC.2014.7039438.
[15] L. Ryba, J. Dokoupil, A. Voda, and G. Besancon, "Adaptive hysteresis compensation on an experimental nanopositioning platform," *Int. J. Control*, vol. 90, no. 4, pp. 765–778, Apr. 2017, doi: 10.1080/00207179.2016.1214874.
[16] X. Tan and J. S. Baras, "Adaptive identification and control of hysteresis in smart materials," *IEEE Trans. Autom. Control*, vol. 50, no. 6, pp. 827–839, Jun. 2005, doi: 10.1109/TAC.2005.849215.
[17] G. Tao and P. V. Kokotović, *Adaptive Control of Systems with Actuator and Sensor Nonlinearities*. New York, NY, USA: Wiley, 1996.
[18] X. Fan and R. C. Smith, "Model-based L_1 adaptive control of hysteresis in smart materials," in *Proc. 47th IEEE Conf. Decis. Control*, Cancun, Mexico, 2008, pp. 3251–3256, doi: 10.1109/CDC.2008.4739393.
[19] X. Chen, T. Hisayama, and C.-Y. Su, "Adaptive control for uncertain continuous-time systems using implicit inversion of Prandtl–Ishlinskii hysteresis representation," *IEEE Trans. Autom. Control*, vol. 55, no. 10, pp. 2357–2363, Oct. 2010, doi: 10.1109/TAC.2010.2053737.
[20] A. Esbrook, X. Tan, and H. K. Khalil, "Control of systems with hysteresis via servocompensation and its application to nanopositioning," *IEEE Trans. Control Syst. Technol.*, vol. 21, no. 3, pp. 725–738, May 2013, doi: 10.1109/TCST.2012.2192734.
[21] K. Kuhnen and H. Janocha, "Adaptive inverse control of piezoelectric actuators with hysteresis operators," in *Proc. Eur. Control Conf.*, Karlsruhe, Germany, 1999, pp. 791–796, doi: 10.23919/ECC.1999.7099402.
[22] A. Esbrook, X. Tan, and H. Khalil, "A robust adaptive servocompensator for nanopositioning control," in *Proc. 49th IEEE Conf. Decis. Control*, Atlanta, GA, USA, 2010, pp. 3688–3693, doi: 10.1109/CDC.2010.5717286.
[23] Y. Al-Nadawi, X. Tan, and H. Khalil, "An adaptive conditional servocompensator design for nanopositioning control," in *Proc. IEEE 56th Annu. Conf. Decis. Control*, Melbourne, Australia, 2017, pp. 885–890, doi: 10.1109/CDC.2017.8263771.
[24] M. Rakotondrabe, K. Rabenorosoa, J. Agnus, and N. Chaillet, "Robust feedforward-feedback control of a nonlinear and oscillating 2-DOF piezocantilever," *IEEE Trans. Autom. Sci. Eng. (from July 2004)*, vol. 8, no. 3, pp. 506–519, Jul. 2011, doi: 10.1109/TASE.2010.2099218.
[25] K. K. Leang and S. Devasia, "Feedback-linearized inverse feedforward for creep, hysteresis, and vibration compensation in AFM piezoactuators," *IEEE Trans. Control Syst. Technol.*, vol. 15, no. 5, pp. 927–935, Sep. 2007, doi: 10.1109/TCST.2007.902956.
[26] B. Jayawardhana, H. Logemann, and E. Ryan, "PID control of second-order systems with hysteresis," *Int. J. Control*, vol. 81, no. 8, pp. 1331–1342, Aug. 2008, doi: 10.1080/00207170701772479.
[27] J. Nealis and R. Smith, "Model-based robust control design for magnetostrictive transducers operating in hysteretic and nonlinear regimes," *IEEE Trans. Control Syst. Technol.*, vol. 15, no. 1, pp. 22–39, Jan. 2007, doi: 10.1109/TCST.2006.883235.
[28] M. Al Janaideh, S. Rakheja, and C.-Y. Su, "An analytical generalized Prandtl–Ishlinskii model inversion for hysteresis compensation in micropositioning control," *IEEE/ASME Trans. Mechatronics*, vol. 16, no. 4, pp. 734–744, Jul. 2010, doi: 10.1109/TMECH.2010.2052366.
[29] K. Kuhnen, "Modeling, identification and compensation of complex hysteretic nonlinearities: A modified Prandtl–Ishlinskii approach," *Eur. J. Control*, vol. 9, no. 4, pp. 407–418, Jan. 2003, doi: 10.3166/ejc.9.407-418.
[30] J. Zhang, E. Merced, N. Sepulveda, and X. Tan, "Modeling and inverse compensation of hysteresis in vanadium dioxide using an extended generalized Prandtl–Ishlinskii model," *Smart Mater. Struct.*, vol. 23, no. 12, Oct. 2014, Art. no. 125017, doi: 10.1088/0964-1726/23/12/125017.
[31] J. Ma, L. Tian, Y. Li, Z. Yang, Y. Cui, and J. Chu, "Hysteresis compensation of piezoelectric deformable mirror based on Prandtl–Ishlinskii model," *Opt. Commun.*, vol. 416, pp. 94–99, Jun. 2018, doi: 10.1016/j.optcom.2018.02.001.
[32] F. Stefanski, B. Minorowicz, J. Persson, A. Plummer, and C. Bowen, "Non-linear control of a hydraulic piezo-valve using a generalised Prandtl–Ishlinskii hysteresis model," *Mech. Syst. Signal Process.*, vol. 82, no. 1, pp. 412–431, Jan. 2017, doi: 10.1016/j.ymssp.2016.05.032.
[33] M. Al Janaideh, M. Rakotondrabe, and O. Aljanaideh, "Further results on hysteresis compensation of smart micropositioning systems with the inverse Prandtl–Ishlinskii compensator," *IEEE Trans. Control Syst. Technol.*, vol. 24, no. 2, pp. 428–439, Mar. 2016, doi: 10.1109/TCST.2015.2446959.
[34] M. Al Janaideh and O. Aljanaideh, "Further results on open-loop compensation of rate-dependent hysteresis in a magnetostrictive actuator with the Prandtl–Ishlinskii model," *Mech. Syst. Signal Process.*, vol. 104, pp. 835–850, May 2018, doi: 10.1016/j.ymssp.2017.09.004.
[35] S. Xie, J. Mei, H. Liu, and Y. Wang, "Hysteresis modeling and trajectory tracking control of the pneumatic muscle actuator using modified Prandtl–Ishlinskii model," *Mechanism Mach. Theory*, vol. 120, pp. 213–224, Feb. 2018, doi: 10.1016/j.mechmachtheory.2017.07.016.
[36] O. Aljanaideh, M. Miyasaka, and B. Hannaford, "Integrated asymmetric stop operator based model for strain stress hysteresis characteristics of cable driven robots loaded longitudinally," in *Proc. IEEE/RSJ Int. Conf. Intell. Robots Syst.*, Vancouver, BC, Canada, 2017, pp. 2543–2548, doi: 10.1109/IROS.2017.8206075.
[37] L. Riccardi, D. Naso, B. Turchiano, H. Janocha, and D. K. Palagachev, "On PID control of dynamic systems with hysteresis using a Prandtl–Ishlinskii model," in *Proc. Amer. Control Conf.*, Montreal, QC, Canada, 2012, pp. 1670–1675, doi: 10.1109/ACC.2012.6315107.
[38] Y. K. Al-Nadawi, X. Tan, and H. K. Khalil, "Inversion-free hysteresis compensation via adaptive conditional servomechanism with application to nanopositioning control," *IEEE Trans. Control Syst. Technol.*, vol. 29, no. 5, pp. 1922–1935, Sep. 2021, doi: 10.1109/TCST.2020.3026018.
[39] A. H. El-Shaer, M. Al Janaideh, P. Krejčí, and M. Tomizuka, "Robust performance enhancement using disturbance observers for hysteresis compensation based on generalized Prandtl–Ishlinskii model," *J. Dyn. Syst., Meas., Control*, vol. 135, no. 5, pp. 1–13, Sep. 2013, doi: 10.1115/1.4023762.
[40] D. Chowdhury, Y. K. Al-Nadawi, and X. Tan, "Dynamic inversion-based hysteresis compensation using extended high-gain observer," *Automatica*, vol. 135, pp. 1–9, Jan. 2022, doi: 10.1016/j.automatica.2021.109977.
[41] M. A. Janaideh, R. Naldi, L. Marconi, and P. Krejčí, "A hybrid system for a class of hysteresis nonlinearity: Modeling and compensation," in *Proc. 51st IEEE Conf. Decis. Control*, Maui, HI, USA, 2012, pp. 5380–5385, doi: 10.1109/CDC.2012.6426019.
[42] P. Krejčí, *Hysteresis, Convexity and Dissipation in Hyperbolic Equations*. Tokyo, Japan: Gakkotosho, 1996.
[43] A. Visintin, *Differential Models of Hysteresis*, vol. 111. Berlin, Germany: Springer-Verlag, 2013.
[44] M. A. Janaideh and P. Krejčí, "A rheological model for the rate-dependent Prandtl–Ishlinskii model," in *Proc. 52nd IEEE Conf. Decis. Control*, Firenze, Italy, 2013, pp. 6646–6651, doi: 10.1109/CDC.2013.6760941.
[45] P. Krejčí and K. Kuhnen, "Inverse control of systems with hysteresis and creep," *IEE Proc.-Control Theory Appl.*, vol. 148, no. 3, pp. 185–192, May 2001, doi: 10.1049/ip-cta:20010375.
[46] M. Al Janaideh, R. Xu, and X. Tan, "Adaptive estimation of play radii for a Prandtl–Ishlinskii hysteresis operator," *IEEE Trans. Control Syst. Technol.*, vol. 29, no. 6, pp. 2687–2695, Nov. 2021, doi: 10.1109/TCST.2020.3046019.
[47] J. Zhang, E. Merced, N. Sepúlveda, and X. Tan, "Optimal compression of generalized Prandtl–Ishlinskii hysteresis models," *Automatica*, vol. 57, pp. 170–179, Jul. 2015, doi: 10.1016/j.automatica.2015.04.012.
[48] K. Kuhnen, "Compensation of parameter-dependent complex hysteretic actuator nonlinearities in smart material systems," *J. Intell. Mater. Syst. Struct.*, vol. 19, no. 12, pp. 1411–1424, Dec. 2008, doi: 10.1177/1045389X08089690.